Abstract

SOOD, AVNEET. A New Monte Carlo Assisted Approach to Detector Response Functions. (Under the direction of Dr. Robin P. Gardner.)

The physical mechanisms that describe the components of NaI, Ge, and SiLi detector response have been investigated using Monte Carlo simulation. The mechanisms described focus on the shape of the Compton edge, the magnitude of the flat continuum, and the shape of the exponential tails features. These features are not accurately predicted by previous Monte Carlo simulation. Probable interaction mechanisms for each detector response component is given based on this Monte Carlo simulation.

Precollision momentum of the electron is considered when simulating incoherent scattering of the photon. The description of the Doppler broadened photon energy spectrum corrects the shape of the Compton edge. Special attention is given to partial energy loss mechanisms in the frontal region of the detector like the escape of photoelectric and Auger electrons or low-energy X-rays from the detector surface. The results include a possible physical mechanism describing the exponential tail feature that is generated by a separate Monte Carlo simulation. Also included is a description of a convolution effect that accounts for the difference in magnitude of the flat continuum in the Monte Carlo simulation and experimental spectra. The convolution describes an enhanced electron loss. Results of these applications are discussed.

A New Monte Carlo Assisted Approach to Detector Response Functions

by

Avneet Sood

A dissertation submitted to the Graduate Faculty of
North Carolina State University
in partial fulfillment of the
requirements for the Degree of
Doctor of Philosophy

Nuclear Engineering

Raleigh, North Carolina

3 April 2000

Approved By:

Prof. Robin P. Gardner, Chair	Prof. Paul J. Turinsky
Prof. Robert E. White	Prof. Robert E. Funderlic

Biography

Avneet Sood was born in Greensboro, NC in June 1972 to Vijay and Bindu Sood and is the first of four children. He was educated in public schools beginning in Madison, NC. He began his college career at North Carolina State University in 1990, finishing with a Bachelor of Science degree in nuclear engineering and a Bachelor of Science degree in mechanical engineering. In May 1994 he began his graduate studies in nuclear engineering and continued until the completion of his doctorate. He is beginning his career with Los Alamos National Laboratory in New Mexico.

Acknowledgments

The Department of Nuclear engineering at North Carolina State University has been my home for the past ten years. I have truly enjoyed knowing all of the fine faculty and staff in the department. I will truly miss the closeness of this department. Professor Robin Gardner has been especially important in guiding my development. His insight and patience has been the key to my success.

Along the way, I have made many lifelong friends, too many to name. My success is partly due to these people. Along with them, my family has been the center of my support. Without their sacrifices and encouragement, I would not have been able to complete my degree. I will always be indebted to them.

Contents

List of Figures

List of Tables

1 Introduction

Detector response functions (drf's) are becoming more and more useful in radiation detection for spectrometry purposes. Specifically, Monte Carlo models used to predict incident photon spectra are applied in conjunction with the detector response function to translate photons incident on the detector to a pulse-height spectrum. The detector response function is defined as the pulse-height distribution for an incident monoenergetic gamma or X ray usually denoted $R(E', E)$ where E' is the pulse-height energy and E is the incident gamma- or X-ray energy. The drf is a probability distribution function (pdf) which has the properties that it is always larger than or equal to zero over its entire range and integrates over all E' to unity.

Detector response functions defined in this manner are rarely obtained directly by experiment since features are almost always present in experimental spectra that are not a part of this function. As an example, features from interactions in the shielding or source like a 180° backscatter gamma ray peak or a 0.511 MeV annihilation photon peak are not part of the drf as defined here. Detector response functions determined experimentally are more appropriately described as library spectra because they include the effects of interactions with surrounding materials and variations in the source.

General purpose Monte Carlo codes such as MCNP and ITS are now accurate enough to be used to simulate detector response by simulating as much of a detector response function as possible. In principle, one could use Monte Carlo simulation entirely to produce drf's if all of the pertinent detector characteristics were known

exactly. However, there are many features of interest that cannot be determined and cannot be simulated. Features like the detector imperfections within the crystal, which significantly affect the flat continuum, are nearly impossible to determine. The same is true for determining the standard deviation of the Gaussian detector resolution and the extent of the exponential tails. Since generating these characteristics by Monte Carlo is not a practical solution, instead Monte Carlo simulation can be used to determine the extent of the full energy peak, the Compton continuua, and the annihilation photon and X-ray escape peaks. We propose to use Monte Carlo simulation to obtain these features and then augment these results with separate simple programs that are used to match a limited number of experimental single-energy spectral data for the three features: (1) Gaussian standard deviation of the full energy peak (and entire spectrum), (2) exponential tail(s), and (3) flat continuua.

Once the drf is developed, it is very useful in further Monte Carlo simulation because it can be used with an incident particle distribution to produce a pulse-height distribution. Detector response functions used in this manner assumes that the response is independent of angle of incidence and point of entry. Specificially, the assumptions require the ratio of the detector length to detector diameter, L/D,to be close to unity and that there is no collimation of the source. Under these assumptions, the drf can be used to automatically smooth the original incident spectrum considerably and eliminate the need for following particles inside the detector. This allows one to use standard flux tallies with any variance reduction technique in a Monte Carlo code rather than having to perform the simulation in analog mode.

2 Review of Previous Work

There are three basic approaches to obtaining detector response functions. They are identified by Gardner, Yacout, Zhang, and Verghese (1986):

- Experimental: where one obtains the response in matrix form from a large number of measured monoenergetic spectra and interpolates for other energies.
- Monte Carlo: where one generates response functions by simulation for a large number of monoenergetic spectra and interpolates for other energies.
- Semi-empirical: where one determines an analytic model and uses least-squares fits to a smaller number of single energy results and then generalizes these results with energy to provide a continuous model.

The first approach can be applied directly, but has the disadvantage of requiring a large number of difficult experimental measurements under standard conditions as done in a catalogue by Heath (Heath, 1964 and Heath, 1974). Often times there are insufficient single energy samples to generate a complete energy range. The second approach minimizes the amount of experimental work required and gives valuable insight into the actual processes that take place within the detector, but additionally requires very careful analysis and description of the problem for sufficient accuracy. In many cases, the characteristic parameters of the detector are difficult if not impossible to obtain. Also, certain effects still cannot be adequately predicted by Monte Carlo like: (1) the Gaussian standard deviation of the full energy peak (and entire

spectrum), (2) the exponential tail(s), and (3) the flat continuua. The third approach utilizes general physical mechanisms that lead to the simple shapes of the various features. However, this method does not give much insight into the physical processes that take place inside of the detector. In previous work, there is insufficient accuracy in the sharpness of the Compton edge with further discrepancies in the flat continuum and exponential tails for low and high energy ranges (Wang, 1996).

There have been many years of effort devoted to generating detector response functions, and, consequently, the literature offers an exhaustive set of references. However, many of these methods concentrate on accurate description of specific features like the photopeak only and do not appear to accurately describe the entire detector response shape to monoenergetic gamma- or X-ray point sources. There is a growing amount of general interest in using all information available from the pulse-height spectra. The present work addresses this growing interest by considering the entire shape of the detector response. Not all of the methods described in the literature are reviewed because a number of references do not influence this work directly and the total number becomes too large. This work reviews some of the more influential methods in generating detector response functions that consider the features of the *entire* spectrum and its shape. For other work not included in this report, see the reference list.

The Center for Engineering Applications of Radioisotopes (CEAR) has a long history of research on detector response functions (drf's). A series of papers (Gardner, Yacout, Zhang, and Verghese, 1986; Jin, Gardner, and Verghese, 1986; and Yacout, Gardner, and Verghese, 1986) outlined the semi-empirical approach that has been

adopted as a standard method for constructing detector response functions. That approach consisted of first identifying a number of separable features that include:

- the full energy Gaussian peak,
- a single Gaussian escape peak due to annihilation photons,
- a double Gaussian escape peak due to annihilation photons,
- one or two exponential tails on the low-energy side of the full energy peak,
- a flat continuum that ranges from zero to the full energy peak,
- a Compton scattering continuum from zero to the full energy peak (primarily from zero to the Compton 'edge'),
- a Compton scattering continuum between the first and second escape peaks due to the Compton scattering of one of the annihilation photons, and
- X-ray escape peaks from detector component elements such as Ge, Si, and I.

These features are shown in Figures 1 and 2 for Ge and Si(Li) detectors, respectively (Gardner, 1986).

The semi-empirical approach consisted of a least-squares fitting of these features for single gamma-ray-energy radioisotope sources or for single element X-ray energies for a range of gamma- or X-ray energies. The individual parameter values for each energy could be fit to simple functions of energy (such as polynomials) to provide a general detector response function (drf). This approach was useful because each of the features identified could be expressed with relatively simple analytical functions.

The most complex was the Compton continua which were fit for gamma-rays incident on Ge detectors with one, two, or three Compton scatters. Analytical expressions derived using approximations to the scattered photon physics were obtained for the three Compton scatters by using the Klein-Nishina cross section and one and two integrations of it. This could be used for the relatively small Ge detector (39%) because one could neglect the variable attenuation of the Compton scattered photons escaping from the detector. In general one cannot neglect this variation for large detectors. Consequently, the integrations cannot be performed that yield analytical expressions for large detectors.

This approach was pursued for both the Ge detector for gamma rays (Lee, et al, 1987a, 1987b) and for the Si(Li) detector for X rays (He, et al , 1990). A number of things were learned about these drf's and this approach during that time. However, a complete study using a number of detectors was not done. One of the things learned was that the flat continuum was larger than is predicted by electron losses from the detector surface. In some cases this was as much as an order of magnitude. It is believed that this is due to imperfections within the detector that cause additional charge losses. The exponential tails are believed to be due to Auger electron losses to detector windows and "dead" layers (Geretschlager, 1987, Wang, 1992, and Goto, 1993). The features that are specific to each detector (even when detectors are essentially identical in shape and size) are:

- the standard deviation of the Gaussian spreading,
- the extent of the exponential tails, and

- the extent of the flat continuum.

The last two of these are detector specific in part because they involve electron energy losses.

Monte Carlo simulation appeared potentially useful for producing drf's. A study was performed to simulate ^{3}He spectrometers by Monte Carlo simulation (Choi, Wehring, Gardner, and Verghese, 1986). It was found to work quite well without additional modification. The interest naturally shifted to generating drf's for large NaI detectors. Some of the first work in generating the entire spectra was done by Berger and Seltzer. Other authors produced Monte Carlo codes with improvements in the physics description (Rogers, 1982 and Peplow, 1994).

Some authors have devoted great effort in using Monte Carlo simulation to reproduce specific key features of the detector response function (Geretschlager, 1987, Campbell, 1990, Wang, 1992, and Goto, 1993). While this body of work does not concentrate on the entire spectra, significant attention was given to reproduce features like the photopeak, exponential tails, and K-xray escape peaks for low-energy spectroscopy using SiLi detectors. The importance of modelling the frontal region where there is poor charge collection is signficant was stressed. Several models describing incomplete charge collection were presented. Additionally, the interactions of low-energy physics like Auger electrons and X-ray fluorescence lines were shown to contribute to photopeak shape.

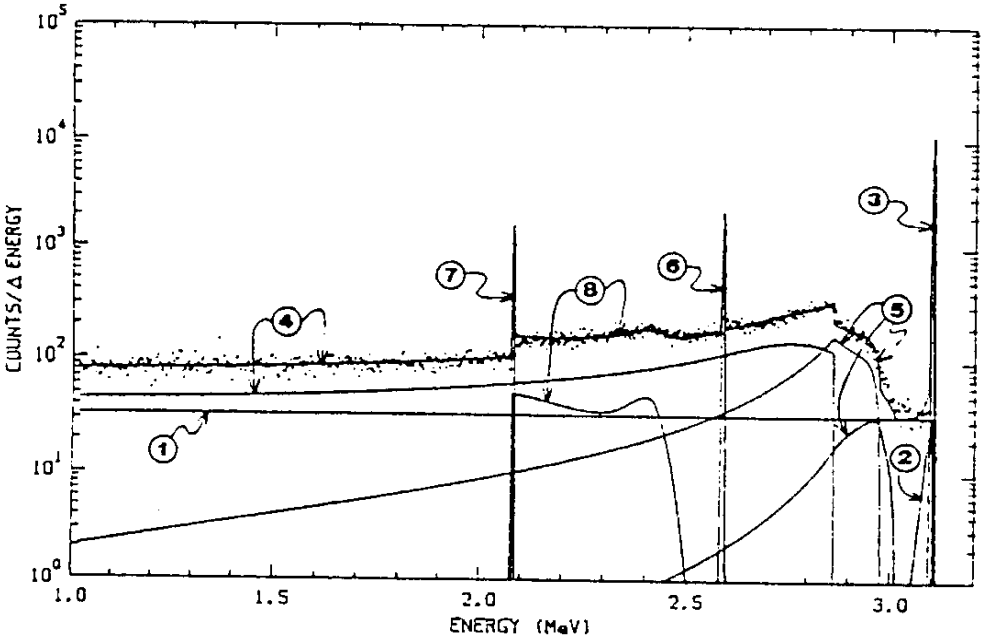

Figure 1: Physical Components of Ge Spectrum: (1) the flat continuum, (2) the exponential tail, (3) the full energy peak, (4) the Compton electron scattering continuum, (5) a continuum between the Compton electron scattering continuum and the full energy peak, (6) the single escape peak, (7) the double escape peak, (8) a small scattering continuum between the single and double escape peaks.

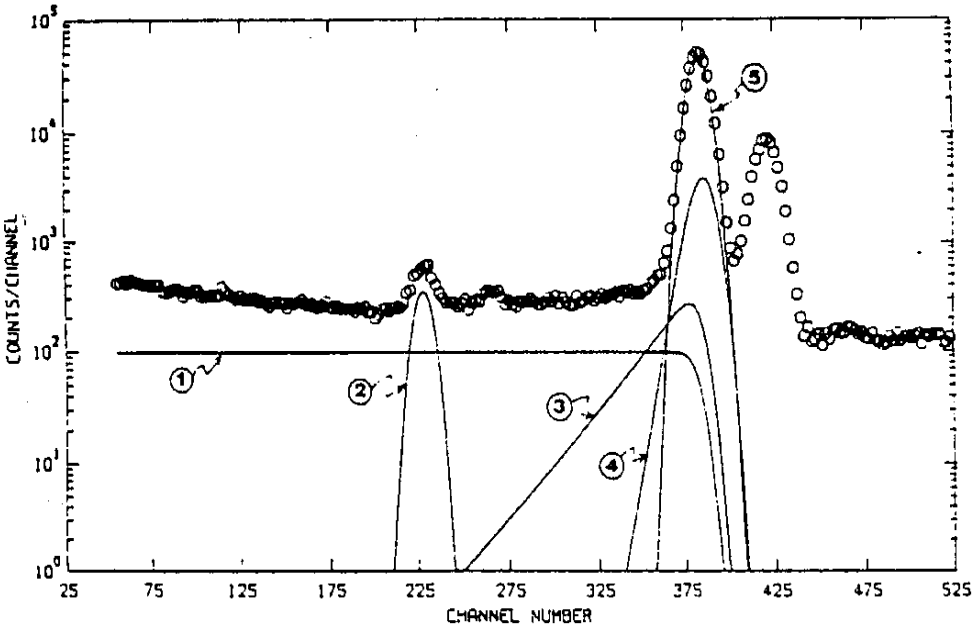

Figure 2: Physical Components of SiLi Spectrum: The spectrum is from an X-ray spectrum of titanium excited by a Cd-109 radioisotope. The features are shown for the Kα X-ray only. The featuresare: (1) the flat continuum, (2) the Si escape peak, (3) the long-term exponential, (4) the short-term exponential, and (5) the full-energy peak.

3 New Approach

Recently studies have been initiated to try to use Monte Carlo simulation to generate as much of the detector response functions as possible. In principle, one could use Monte Carlo simulation entirely to produce drf's if the pertinent detector characteristics are known exactly. However, it is extremely difficult, if not impossible, to determine all the pertinent characteristics. Monte Carlo simulation can be used to determine the extent of the full energy peak, the Compton continuua, and the annihilation photon and X-ray escape peaks. These results can be augmented with separate simple programs that are used to match a limited number of experimental single-energy spectral data for the three features: (1) Gaussian standard deviation of the full energy (and entire spectrum) peak, (2) exponential tail(s), and (3) flat continuua.

Three slight modifications of the previous drf treatment for gamma and X rays have recently been identified and describe the ideas presented in this work. These are:

- the flat continuum comes not only from the full energy peak, but also from all parts of the photon spectrum, including the Compton continuum,
- the shape of gamma- and X-ray pulse-height spectra in semi-conductor detectors is influenced significantly by Doppler broadening, particularly in the spectral region of the Compton scattering continuum, and
- crystal imperfections serve as electron trapping sites, increasing the amount of

incomplete charge collection.

The second effect is seen most clearly in Ge gamma-ray spectra at the Compton edge which is degraded in its sharpness considerably by the Doppler broadening effect. In X-ray spectra it is seen in the Compton backscatter peaks from discrete energy radioisotope excitation sources.

The first and third effects are similar to electron losses from the surface of the detector crystal. Preliminary studies indicated that the entire photon spectrum contributed to the shape of the flat continuum. One of the proposed solutions was to increase the electron leakage artificially by increasing the electron range thus simulating charge loss due to imperfections or electron channeling effects. This could be included in the Monte Carlo simulation by modifying the density of the material for the electron when an electron is created. Alternatively, one could simply reduce the photopeak by a specified fraction and distribute it to the rest of the spectrum. This offers the advantage of a convolution after the Monte Carlo simulation that is particular to a specific detector.

These convolution or spreading effects must be implemented to obtain the final pulse-height spectra. Since they are presently not in the existing general purpose codes like MCNP and ITS, it is important to be able to implement them after and outside of a normal Monte Carlo simulation. A program has been written to simulate the increased electron leakage by applying a fraction of the photons that deposit their full energy and simply spreading them equally over the entire spectrum below the energy of interest.

4 Experimental Data

Most of the experimental digital library data was obtained from R.L. Heath for a number of single gamma-ray energies that were reported in his original NaI Gamma-Ray Spectrum Catalogue (Heath, 1964) and Gamma-Ray Spectrum Catalogue for Ge(Li) and SiLi (Heath, 1974). Other data were generated at NCSU for comparison of methodology. These data were very carefully taken under standard conditions and represent the best benchmarked data available. It is important to note, however, that any data taken in this manner contain a few features that are not part of the detector response function as previously defined. This includes the backscatter peak that is due to 180-degree scatters from the standard shield used by Heath and the 0.511 MeV peak from annihilation photons that also come from the shield. By the original definition of the drf, only the features that come directly from the incident monoenergetic gamma- or X-ray are a part of the drf. In the present case the standard shield used by Heath is included in the Monte Carlo calculations so that these additional features will be included in the predictions. So in this case we are obtaining standard gamma-ray library spectra instead of detector response functions. It is reasoned that if we can simulate these standard spectra accurately then we should be able to simulate the detector response functions just as accurately by simply removing the shield from the Monte Carlo simulation.

5 DRF Code Development

General pupose codes like MCNP, ITS, and EGS4 can be used for calculating

detector response functions. However, additional tallies must be specifically created to allow the investigation of the components of the detector response function. It is useful to develop specific purpose codes that allow the user to concentrate on specific physical mechanisms that occur because these very specific tally features are not available. The specific purpose codes are also useful analysis tools because the general purpose codes only allow analog simulation when calculating the pulse-height tally; the user is not able to see the effect of less probable events on the detector response without a very long simulation time.

To address the need of adequate analysis tools, a Monte Carlo code, CEARDRF, has been developed to simulate the response of a bare Si(Li), Ge, or NaI detector crystal to a monoenergetic point source. The unique feature of this code is that the individual components of the detector response function are specifically tallied and produced separately. Using this technique, the contribution to the pulse height tally from physical mechanisms such as secondary electron escape and dead layer losses can be studied in great detail. Distributions of these physical mechanisms can be produced directly from the simulation. This will replace any of the approximations introduced in semi-empirical models such as neglecting attenuation in the contribution from multiple Compton scattering. This feature allows differences in experimental and predicted responses to be characterized by observing the contribution of the individual components.

5.1 Calculating the response function

The Monte Carlo calculation includes basic gamma-ray interactions: photoelectric absorption, incoherent scattering, and pair production. Rayleigh scattering is not included. Cross sections are generated from the general purpose Monte Carlo code, MCNP (Breismeister, 1997), which uses updated values of Storm and Israel (1967) data. Electrons and positrons produced in the detector include bremsstrahlung production and are transported using a simplified range model. After the beginning of each history, an interaction is forced to occur inside the detector. Once inside the detector, all particles are allowed to leave the detector. Once outside of the detector, the escaped particles do not further contribute to the response function. A description of physical mechanisms in the Monte Carlo simulation is given. Attention is focused on the simplifying assumptions to the detailed physics. Details of the basic photon physics used can be found in any introductory nuclear engineering textbooks like Mayo (1998). Similarly, a complete description of the Monte Carlo principles can be found in texts like Carter and Cashwell (1975).

5.1.1 Photoelectric absorption

Photoelectric absorption of the incident photon will generate photoelectrons with either K-shell Auger electrons and the KLL satellite X-rays, or fluorescence X-rays. The photoelectric absorption generates a K-shell photoelectron that is assumed to be emitted isotropically with kinetic energy equal to the difference in incident energy and K-shell binding energy. Once the K-shell vacancy is created, it may be de-excited

by the simultaneous emission of an L-shell Auger electron and the associated satellite X-rays or by the emission of a K_α or K_β fluorescence X-ray. The sum of the energies in the secondary emission must equal the total binding energy of the K-shell vacancy. As atomic number increases, the probability of the Auger effect decreases, thereby increasing the probability of X-ray fluorescence emission. The detector materials under consideration vary up to a Z of 32. All data for the Auger and fluoresence events comes from Krause (1979) and Scofield (1974).

The Auger electron and satellite X-rays are assumed to be emitted isotropically. Only the KLL satellite X-rays are considered because of the dominant probability of emission and intensity over other lines. Previous work by He et al (1990) indicate the importance of Auger electrons and satellite X-rays when describing detector response by semi-empirical fitting methods.

Fluorescence X-rays are also assumed to be emitted isotropically. The allowed fluorescence X-rays are K_α or K_β emission. The K_α emission is simultaneously followed by an associated L_α X-ray. The remaining energy (of a nearly 100 eV) from a K_β emission is deposited locally. Again, these fluorescence X-rays were chosen due to their dominant emission probabilities and intensities.

5.1.2 Incoherent scattering

Incoherent scattering of the incident photon can occur with a bound electron in a shell of the detector material and will generate a Compton electron and a scattered photon. Electron binding effects become important when the photon energy is near a few hundred keV. The result of this binding effects on the angle and energy of the

scattered photon must be taken into account for accurate simulation of low-energy photon transport. The effect of the bound electron on the scattered photon angular distribution appears as a reduction in the total scattering cross section in the forward direction. The electron binding effect on the scattered photon's energy distribution appears as a broadening of the energy spectrum due to the precollision momentum of the electron.

Since incoherent scattering is an important interaction mode for low-energy photons, consideration of the precollision motion of the electron for incoherent scattering, called the Doppler effect, is important for accurately simulating the transport of photons. Since the treatment modifies the angular and energy distribution of a scattered photon, it will modify the calculation of the mean free path of a photon through a material. The most dramatic effect appears in the pulse height spectra in the prediction of energy distribution in the region near the Compton edge and the associated continuum. This can be seen when comparing Monte Carlo simulated results and experimental results. Evidence of the Doppler broadening has been documented very well in the past few years (Namito, 1993 and Lee, 1999). Direct comparison of experimental and calculated pulse height spectra demonstrates the dramatic difference in the Compton region. This can be seen in Figure 3 from Namito's implementation of Doppler broadening with a linearly polarized mono-energetic beam in EGS4. Figure 3 also shows a comparison of MCNP with the addition of Doppler broadening. The effect of Doppler broadening is clearly seen in the shape of the Compton scatter region. The results do not match the EGS4 results of Namito because MCNP does not implement linearly polarized photons. As incident photon energy increases, the

effect of the precollision momentum of the electron decreases the Doppler broadening effect on the predicted pulse height spectra.

The modification of the angular distribution has been accounted for by several Monte Carlo transport codes by using an incoherent scattering function multiplying the total cross section. The effect of the incoherent scattering function is to decrease the Klein-Nishina cross section per electron more extremely in the forward direction for low-energy and for high Z, independently. However, the broadening of the scattered photon energy is not treated, as of yet, by many current versions of general purpose Monte Carlo transport codes like ITS, EGS4, and MCNP. The first inclusion of the Doppler broadened energy in a Monte Carlo code that appears in the literature was by Felsteiner, Pattison and Cooper (1974) with the purpose to correct experimental Compton profiles for the effect of multiple scattered photons in their measurement sample. A standard method of implimenting Doppler broadening was set forth by Namito, Ban, and Hirayama (1994) in an improved version of EGS4. Their paper provides a discussion of the formulas for describing the Doppler broadening, incoherent scattering function, and total incoherent cross section of a low-energy photon.

The method of calculation used here is the same as described by Namito, et al (1994) and has been used locally at NCSU by Lee, Ao, and Gardner (1999) in their specific purpose X-ray Fluorescence code, CEARXRF. The same treatment is adopted with CEARDRF and is included in a local version of MCNP4B by a patch.

When a photon undergoes an incoherent scatter in the Monte Carlo simulation, the cosine of the exit angle, θ, is sampled from a modified Klein-Nishina differential

cross section:

$$\frac{d\sigma_{inc}}{d\Omega}(\theta,\phi) = \frac{d\sigma_{KN}}{d\Omega}(\theta,\phi)S(x,Z) \quad (1)$$

where S(x,Z) is the incoherent scattering factor. For any Z, S(x,Z) increases from zero until Z at Z=infinity. The parameter, x, is the inverse length = $\sin(\theta/2)/\lambda$ = $\kappa\alpha\sqrt{1-\mu}$ where κ=10^{-8} mc/(h $\sqrt{2}$) = 29.1445 cm $^{-1}$ and α is the initial photon energy in units of rest mass energy of an electron.

The cosine of the scattering polar angle, μ, is calculated by using Kahn's rejection method which samples the Klein-Nishina formula exactly. The final angle is rejected according to the incoherent scattering function, S(x,Z).

The scattered photon's energy must be determined next by using the shellwise Compton profiles. The Compton profiles are tabulated as a function of the projected precollision momentum of the electon on the momentum transfer vector of the photon. This is described by:

$$p_z = -137\frac{E_i - E_s - E_iE_s(1-\mu)/m_oc^2}{\sqrt{E_i^2+E_s^2-2E_iE_s\mu}} \quad (2)$$

where p_z is in atomic units of $m_oc^2/\bar{h}$, E_i and E_s are the incident and scattered photon energies, respectively. The Compton profiles are related to the incoherent scattering function, S(x,Z) by:

$$S(x,Z) = \sum_k \int_{-\infty}^{p_{z_{max}}} J_k(p_z,Z)dp_z \quad (3)$$

where k refers to the particular electron subshell and $p_{z_{max}}$ is the maximum momentum transferred.

The particular subshell of the electron that interacts with the photon must be chosen. It is picked based on the number of electrons in each subshell. The projected momentum, p_z, is sampled from the Compton profile. The scattered photon energy is calculated by solving p_z for E_s.

5.1.3 Electron transport model

The electron transport model begins with a calculation of the range of the electron. The range equation follows the form:

$$R = \frac{aE^{(b-c\ln(E))}}{\rho} \quad (4)$$

where R is in cm, E is in MeV, and ρ is in g/cm^3. The parameters a, b, and c are empirically determined values. The values as calculated by Pages et al (1972) are a=0.69361, b= 1.1508, and c=0.083893.

The behavior of electron collisions was approximated by assuming that the path begins as a straight line with continuous energy loss by ionization until a major interaction occurs and changes the original direction. Since the electron range is based on an extrapolation of a transmission curve, a modified pdf was created to account for the slightly greater distances (Peplow, 1993). The approximation to the pdf for an electron to travel a distance, d, was made by using:

$$p(d) = (2R/5)(1 + 3d/R) \quad (5)$$

The electron loses energy continuously by ionization collisions moving along this distance. The new energy of the electron due to the ionization collisions can be calculated

by using the range relationship above and solving for the new energy. It is given as:

$$E' = \exp(b/2c - \sqrt{(b^2/4c^2 - 1/c\ln(\rho(R-d)/a))}) \quad (6)$$

The energy deposited in the detector is the difference between the original electron energy and E'.

Changing the direction of the electron results contributes to the radiative energy loss of the electron by the production of bremsstrahlung radiation. Radiative energy loss is dominant for electrons at higher energies while collisional energy loss is dominant for lower energies and is characterized by the stopping power. Instead of modelling the radiative production of bremsstrahlung by use of the stopping power, empirically found values were used instead to match bremsstrahlung spectral shapes generated by the response functions by Berger and Seltzer (1972) and general purpose codes. This approximation was done to increase the computational speed of the specific purpose code while minimizing losses in accuracy. The energy distribution for the bremsstrahlung photon is chosen from values given by Hansen and Fultz (1960). The electron angle is scattered at 90° and the photon is emitted in the original direction of the electron. This procedure has been benchmarked in previous work by Peplow (1993) where comparisons are made with pulse height distributions generated by general purpose codes like ITS and MCNP.

5.2 Benchmarking CEARDRF

The spectra generated by the Monte Carlo code, CEARDRF, was compared with the results from the general purpose code MCNP version 4B2 for bare NaI, Ge, and

SiLi detectors with a monoenergetic point source 10 cm away. Figures 4 - 8 show typical verification comparisons for two single energies for each detector. The slight differences in the Compton valley are due to simplifications in the electron transport and bremsstrahlung production. Computational time with CEARDRF is on the order of 10 to 15 minutes for less than 1% precision in each channel on a Sun Ultra I. MCNP simulation requires 5 hours for the NaI and Ge spectra and up to 10 hours for the low-energy spectra in SiLi detectors for the same precision.

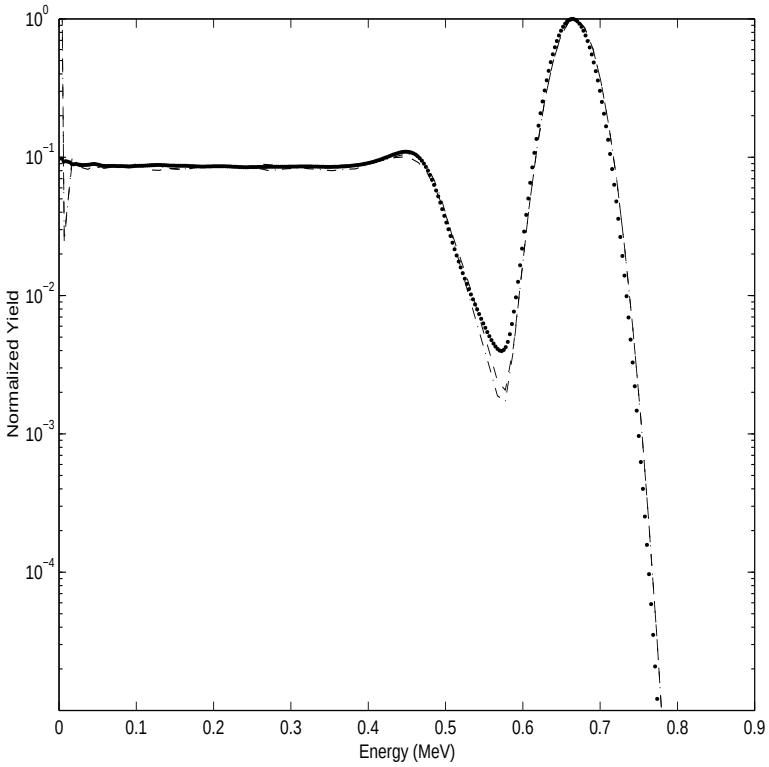

Figure 4: Comparison of NaI Detector Mn-54: CEARDRF (··), MCNP (−−), MCNP with Doppler (−·)

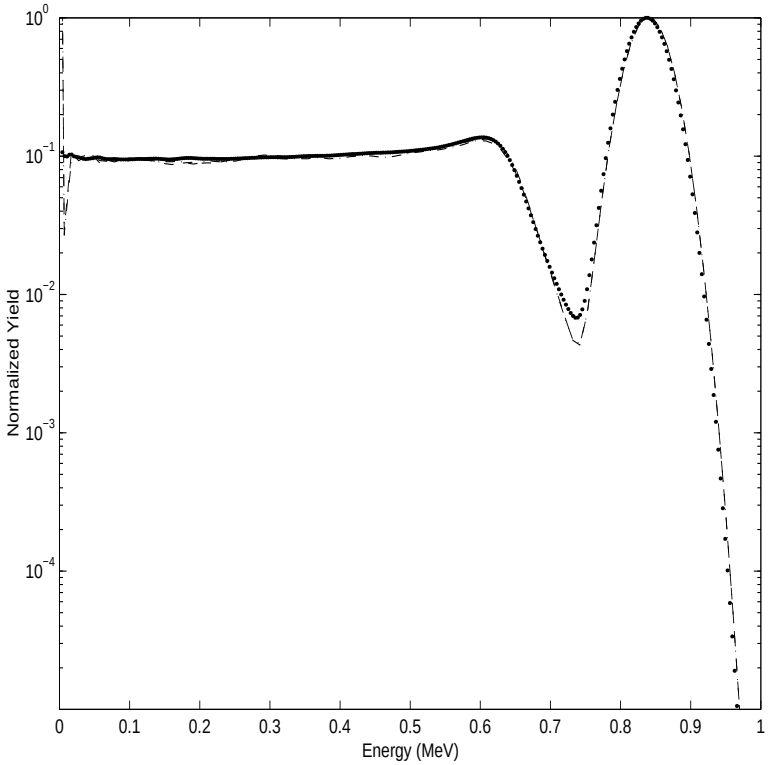

Figure 5: Comparison of NaI Detector Cs-137: CEARDRF (··), MCNP (−−), MCNP with Doppler (−·)

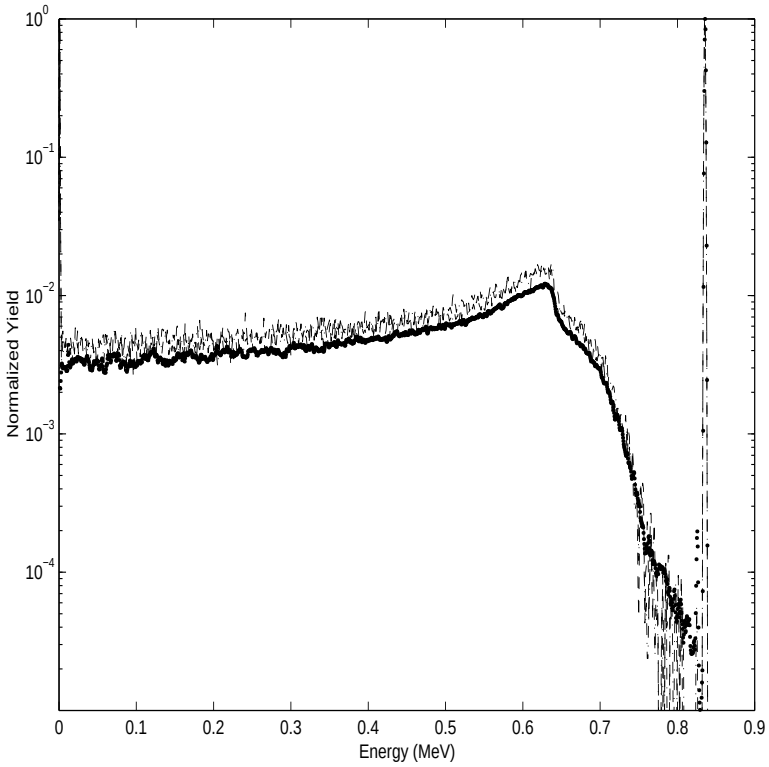

Figure 6: Comparison of Ge Detector Mn-54: CEARDRF (··), MCNP (−−), MCNP with Doppler (−·)

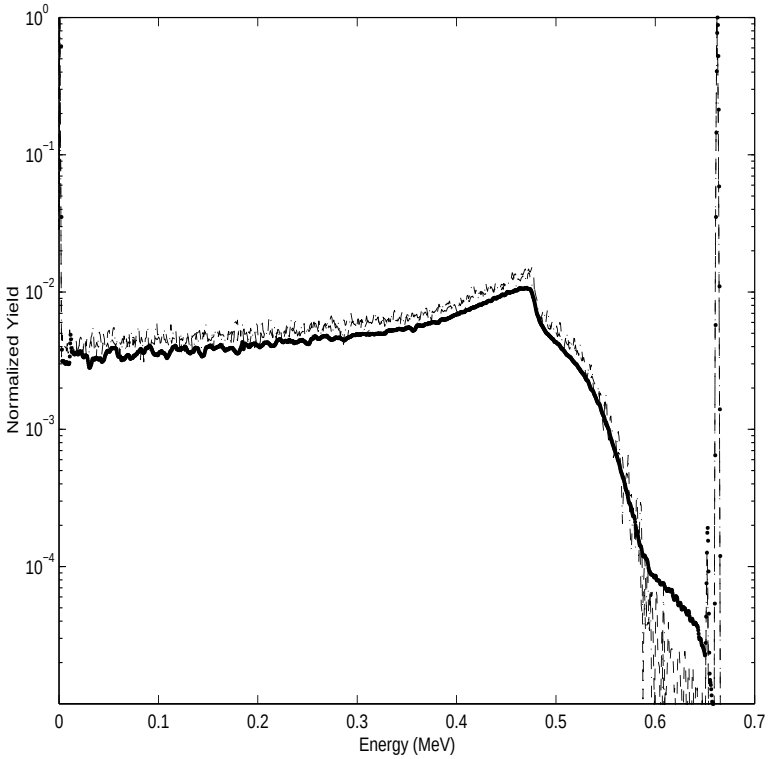

Figure 7: Comparison of Ge Detector Cs-137: CEARDRF (··), MCNP (−−), MCNP with Doppler (−·)

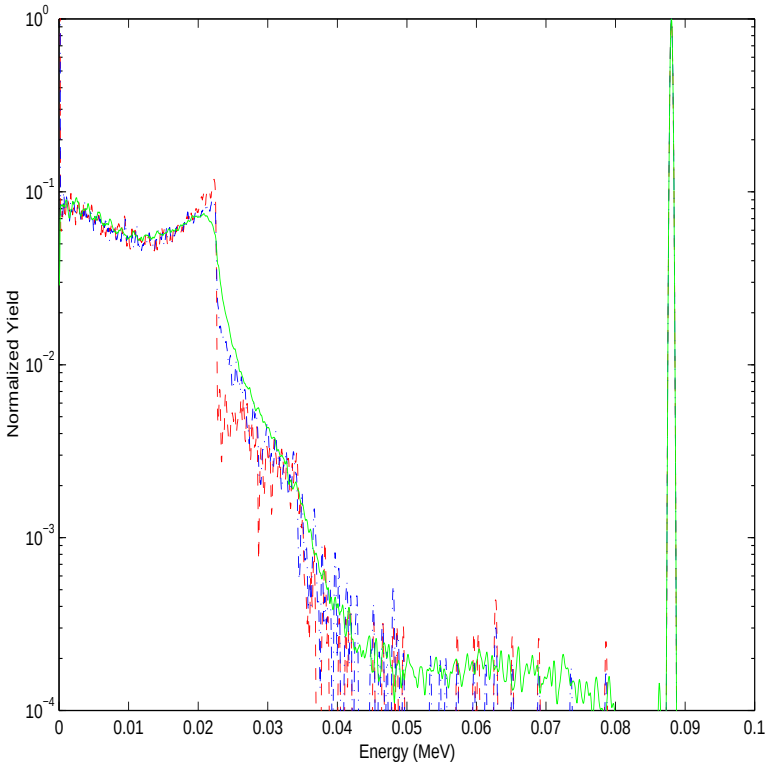

Figure 8: Comparison of SiLi Detector: CEARDRF (··), MCNP (−−), MCNP with Doppler (−·)

6 Components of the Detector Response Function

The components described earlier by Gardner (1986) are derived from analytic descriptions of the physical interactions occuring in the detector. Particular features like the short-term exponential in the SiLi detector response are only evident after other functions have been properly stripped from the spectrum. While the shape of these features have been determined, the physical mechanism describing them has not been clearly identified.

Many of the semi-empirical formulas are derived with simplifying assumptions. An

example is in the multiple Compton scatter component where photon attenuation is ignored. Using Monte Carlo simulation, the individual components can be produced with their true shape limited only by the description of the physics in the simulation. Monte Carlo simulation can be used to generate the components by simply flagging particular interactions when they occur during the normal simulation. For example, the multiple Compton scatter component is generated by counting the number of scatters and determining if the Compton electron deposits its full energy inside the detector and if the Compton scattered photon escapes. At the end of the photon history, the energy deposited from these conditions are tallied separately. Figure 9 shows the basic components of the detector response function. Special attention is required for the exponential tails near the photopeak. These features are described in detail in section 6.2.

The components shown in Figure 9 are obtained directly from the Monte Carlo simulation and convolved with a Gaussian with the appropriate resolution. The features present are:

1. the full energy Gaussian peak,
2. a single Gaussian escape peak due to annihilation photons,
3. a double Gaussian escape peak due to annihilation photons,
4. a flat continuum that ranges from zero to the full energy peak, but is comprised from two physical features,
5. a Doppler broadened Compton scattering continuum broken into first, second,

and third Compton scatters from zero to the full energy peak,

6. a Compton scattering continuum between the first and second escape peaks due to the Compton scattering of one of the annihilation photons, and

7. X-ray escape peaks from detector component elements such as Ge, Si, and I.

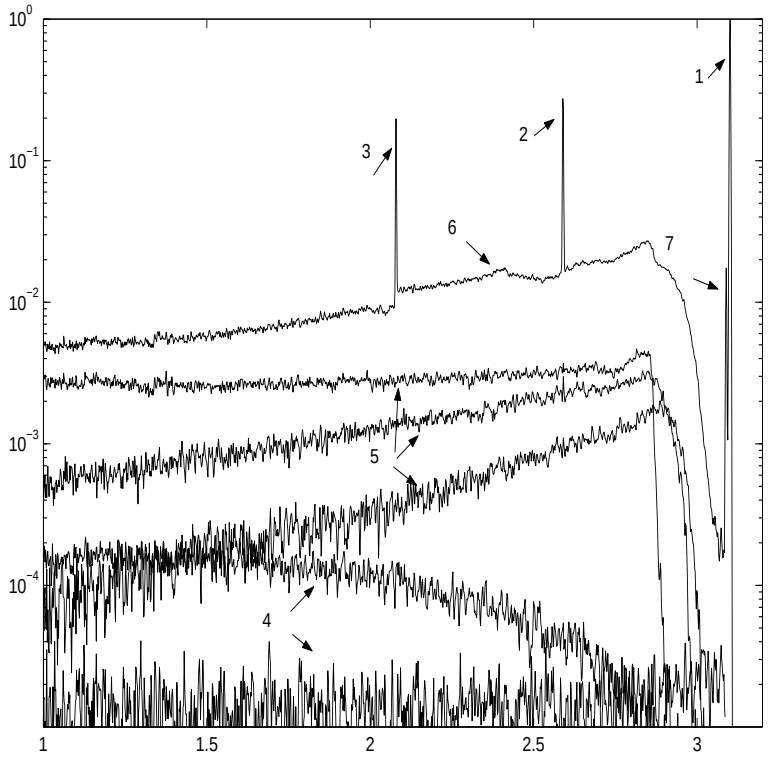

Figure 9: Physical Mechanisms of Detector Response

One of the first distinctions is the shape of the flat continuum. The flat continuum was previously considered as a single feature but is comprised of two different mechanisms that give a flat distribution when combined. This feature is generated by flagging the photoelectron and Compton electron losses from the sides of the detector.

A second distinct feature is the shape of the Compton edge. The Compton edge as predicted by previous Monte Carlo simulation produced a very sharp change in slope indicating a 180^o Compton scatter event. Including the low-energy Doppler effect on the angle and energy of the incident photon produces a shape that matches the experimentally observed shape of the Compton edge. The second, third, and subsequent Compton scatters reflect the effect of the newly implemented low-energy physics. The dominant contribution to the shape of the Compton edge is from the first and second Compton scatters. Notice the change in the shape of the triple Compton scatter contribution.

6.1 Analysis by Region

An important part of this investigation is the ability to concentrate on specific regions of the detector crystal. Previous authors (Geretschlager, 1987, Campbell, 1999, and Goto, 1993) stressed the importance of the frontal region of SiLi detectors. It is assumed that this region is also important for other high resolution detectors like Ge. This region has a significant effect on the shape of the exponential tail behavior in the photopeak. CEARDRF allows the user to force the first interaction within a region defined by the user including any dead layers. The particle weight reduction is accounted for by the ratio of the true and modified probability distribution function describing the forced interaction. The true and modified probability distribution functions used are given as:

$$f_{true}(\rho) = \mu \exp(-\mu\rho) \tag{7}$$

$$f_{mod}(\rho) = \frac{\mu \exp(-\mu\rho)}{\exp(-\mu\rho_{min}) - \exp(-\mu\rho_{max})} \quad (8)$$

$$w_{new} = w_{old}\left[\exp(-\mu\rho_{min}) - \exp(-\mu\rho_{max})\right] \quad (9)$$

where ρ is the distance to interaction and μ is the total interaction probability. The values of ρ_{min} and ρ_{max} determine the limits where the first interaction is forced to occur. All subsequent interactions are allowed to occur within the detector crystal. This would allow the user to investigate the contribution of interactions within a dead layer to specific regions of the detector crystal.

6.2 Exponential Tails

The exponential tail behavior to the left of the photopeak has been well established for semiconductor detectors. The literature has produced a number of studies for SiLi detectors addressing this feature which does not appear in ordinary Monte Carlo simulation but has a significant contribution in low-energy experimental spectra. The low-energy tail has been explained by incomplete charge carrier collection by diffusion towards the surface of the detector crystal, insensitive regions in the frontal layers of the crystal, and by partial energy loss of secondary radiation like Auger electrons, fluorescence X-rays, and photoelectrons. Some work has used a combination of these explainations. Authors have developed general models for describing the charge collection efficiency (Geretschlager, 1987, Wang, 1992, and Goto, 1993) that depend on parameters specific to the semiconductor detector used. These parameters are roughly deduced from precise experiments with these detectors. One of the fundamental parameters of these models is the spatial location of the insensitive region

where the incomplete charge collection is modelled. The work by Goto (1993) applies his incomplete charge collection model over the range of the photoelectron created by the incident photon. Work by Wang and Campbell (1992) examines the effect of moving this boundary on their model of the poorly sensitive region. In reviewing most of the literature, the values vary from 0.1 μm to 1 μm. Monte Carlo simulation usually considers the entire active region of the detector crystal. It has been found in this work as in others that this frontal region has an unusually large contribution to the shape of the exponential tails. This is an important separation of the effect of local properties on the detector response from the bulk properties of the detector crystal.

The specific purpose code, CEARDRF, allows the user to investigate the contribution of any specific region or any insensitive layers to the detector response. As an example, the response can be calculated for a SiLi detector to an 88 keV source with a totally insensitive region, called a dead layer, of thickness equal to 0.1 μm (nearly the range of an KLL Auger electron in silicon). Since the probability of interaction in the dead layer is very small, the first collision is forced to occur in the dead region with the proper particle weight adjustment.

The frontal region of the detector crystal has been found to be unusually signficant to the shape of the photopeak because of the small energy loss mechanisms that occur within the range of the photoelectron. One difficulty with this procedure is determining appropriate lengths of dead layers and frontal regions. The literature suggests dead layers of thickness varing from 0.1 μm to 0.5μm. The frontal region was defined to be the range of the photoelectron. This distance was used because

interactions that occur below the range of the photoelectron will not have any energy loss and any interactions occuring above this range may exhibit minor energy losses from the photoelectron, KLL Auger electron, satellite X-rays, and any fluorescence X-rays. Figure 11 shows the typical shape of the combined effect on the photopeak shape generated when particles are forced within the dead layer and the frontal region of the detector. This shows the contribution of the low-energy Auger electron, satellite X-rays, and fluorescence X-rays on the shape of the photopeak. This shape resembles the combined short-term and long-term exponential peak shapes used with the semi-empirical approach to detector response functions shown in Figures 1 and 2 generated by Gardner (1986). This shape also resembles the experimentally determined KLL Auger electron distribution in Si by Papp, Campbell, et al (1998).

Previous work supports these ideas, however, the magnitude of the contribution in the frontal region has been at least one order of magnitude off. This has been shown in the work by Gardner et al (1986) and is addressed by different authors in many ways. A new approach is suggested to model the loss of secondary radiation in the frontal region. The imperfections in the detector crystal serve as electron trapping sites and thus increase the amount of incomplete charge collection. The resulting effect is similar to electron losses from the surface of the detector crystal. Since this detector characteristic cannot be physically described with much certainty, an approximation must be made. This can be simulated by introducing a 'pseudo' density change in the material properties when an electron is created. Since the reaction rate depends on the product of density and cross section, the reaction rate may be changed by simply modifying the material density instead. Since the frontal

regions of the detector crystal signficantly contribute to the exponential tail, the specific purpose code, CEARDRF, adopts the general shape developed for incomplete charge collection developed by Goto as a pseudo electron density modification. The model given by Goto is based on a one-dimensional electron carrier density model for silicon and looks like:

$$f(z) = 1 - (1 - R)\exp(-Cz) \tag{10}$$

where R controls the rate change in density. The shape is an exponential that quickly reaches saturation. Figure 10 shows the density change as a function of electron generation sites for different R.

Using this density model, several photopeak shapes are generated by including a 0.1 μm dead layer and forcing first collisions within the range of the photoelectron. This distance changes with incident photon energy. The parameter R is changed until the peak shape is matched for a particular detector. Table 1 lists the detector type, incident photon energy, and values of R that generates the photopeak shape.

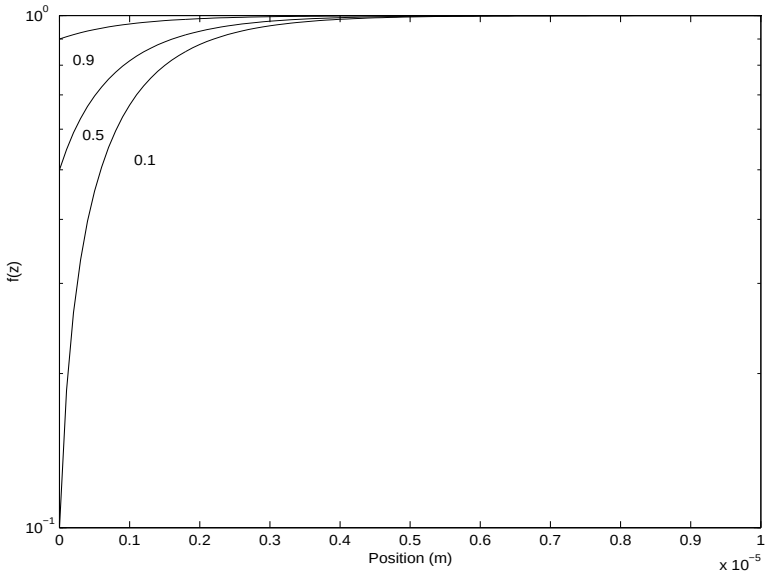

Figure 10: Pseudo-Electron Density Profile

Table 1: Exponential Tail Parameters

Detector Type	Isotope	E (keV)	R
SiLi 1	Fe--55	5.89	0.1
	Mo--93	17.37	0.1
	Cd--109	88.1	0.5
SiLi 2	Cd--109	88.1	0.5
HPGe 1	Cs--137	662	0.5
	Mn--54	835	0.5
HPGe 2	Mn--54	835	0.9
	Cd--109	88.1	0.9

Figures 11-16 show the resulting photopeak shapes. The components of the photopeak are broken into two contributions. The first includes the photoelectron only. The energy due to photoelectron deposition varies from zero to the incident energy less the binding energy. The second contribution includes the Auger electron, satellite X-rays and the Lα fluorescence X-rays. The energy deposited ranges from complete

Auger electron loss to the full energy peak. The Monte Carlo results are convolved with a Gaussian function with the appropriate resolution for each detector. The resulting peak shape is very similar to the combined short term and long term exponential functions generated by the semi-empirical methods. The two components are added together and normalized to the experimental photopeak. It should be noted that the low-energy tailing is not seen in NaI spectra nor will be seen by Monte Carlo simulation. This is due to the larger resolution of the detector.

The small energy losses in the frontal region contribute largely to the exponential tail region. The thickness of this region is estimated to be the sum of the insensitive region and the maximum electron range in silicon or germanium. The K X-rays are allowed to escape but the contribution towards the tail is small.

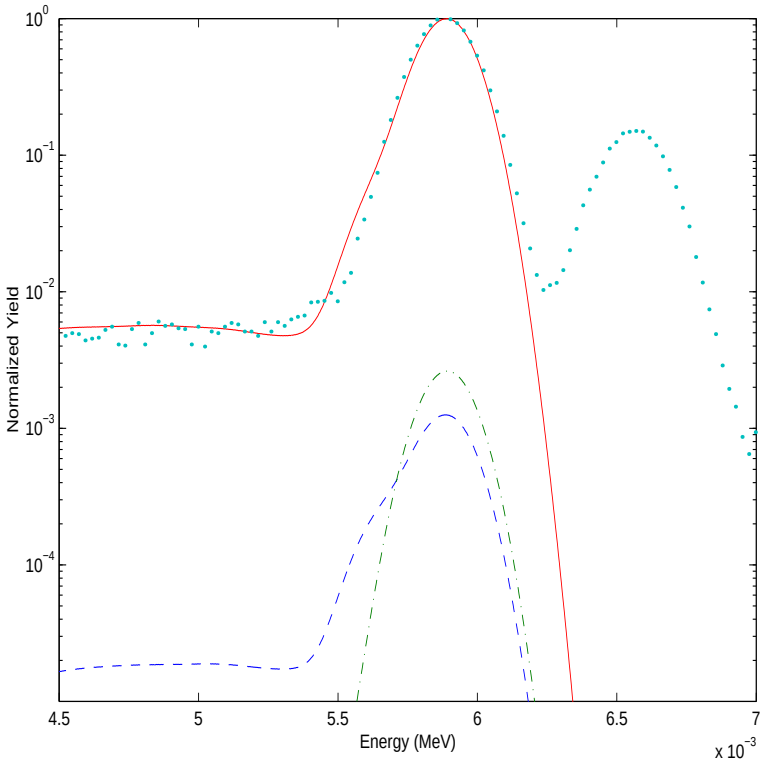

Figure 11: Exponential Tail Components for SiLi #1, Fe-55: Experiment (··), Auger Component (– –), Photoelectron Component (–·)

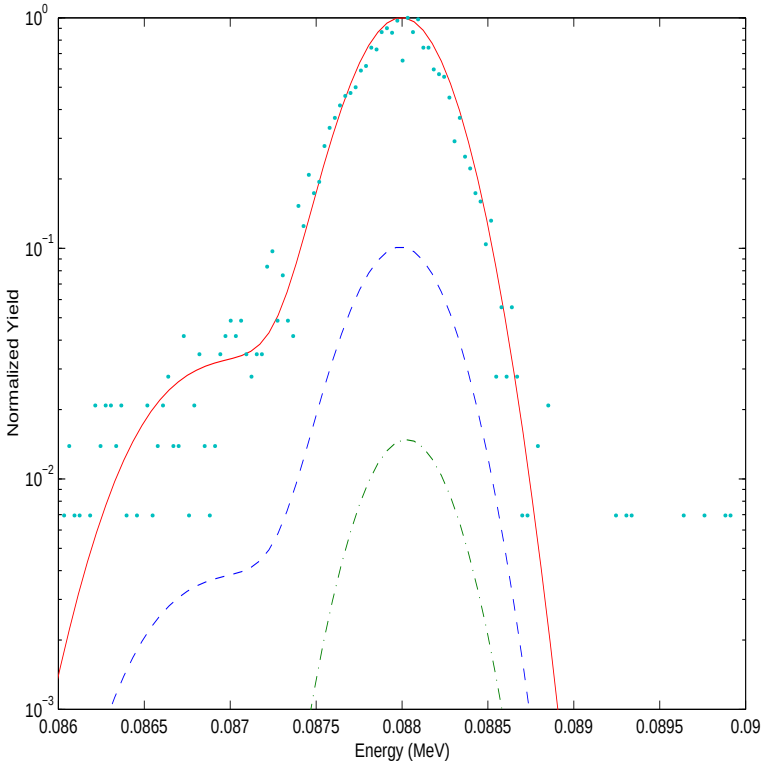

Figure 12: Exponential Tail Components for SiLi #1 Cd-109: Experiment (··), Auger Component (– –), Photoelectron Component (–·)

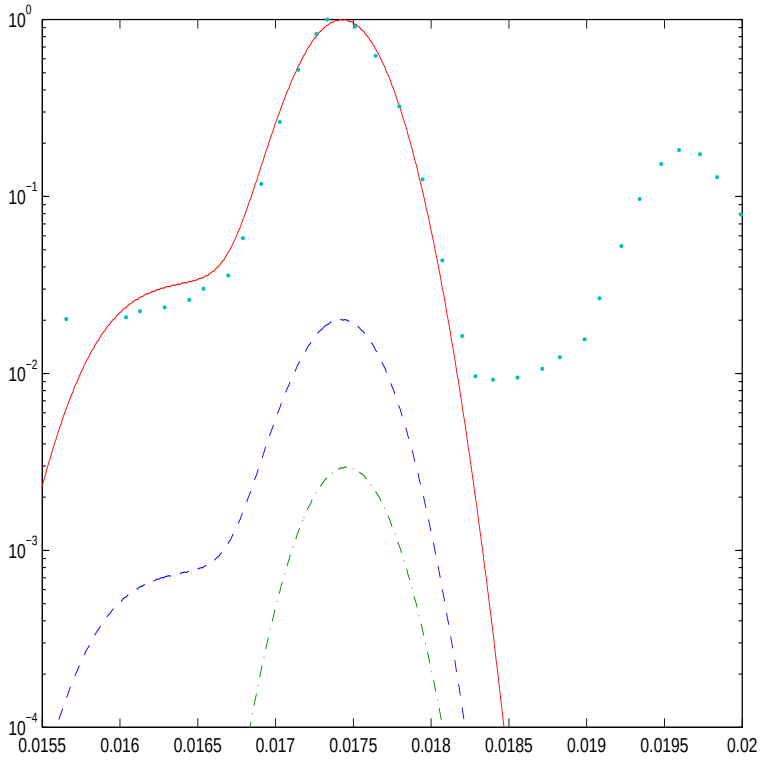

Figure 13: Exponential Tail Components for SiLi #1, Mo-93: Experiment (··), Auger Component (––), Photoelectron Component (–·)

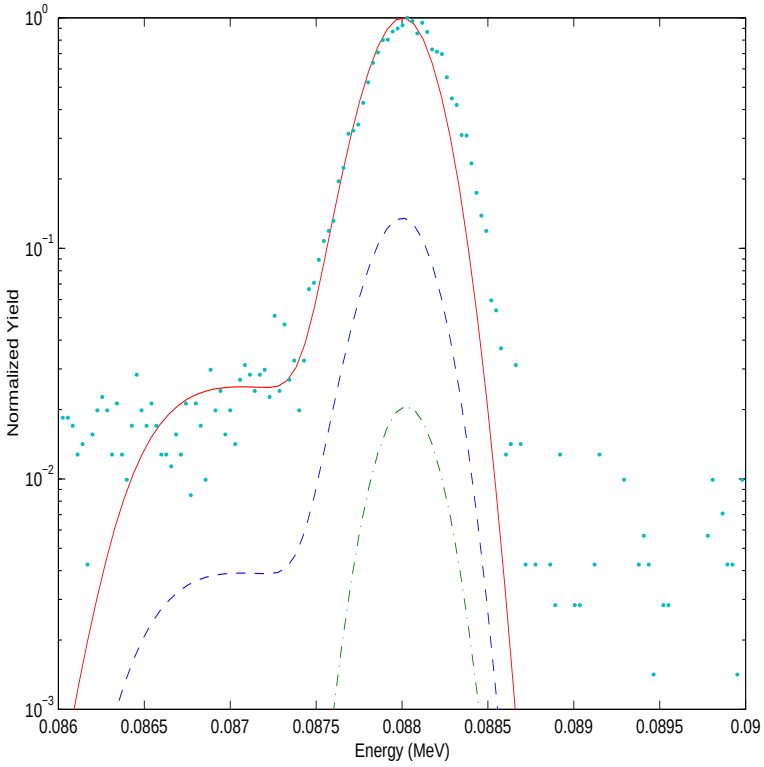

Figure 14: Exponential Tail Components for SiLi #2 Cd-109: Experiment (··), Auger Component (––), Photoelectron Component (–·)

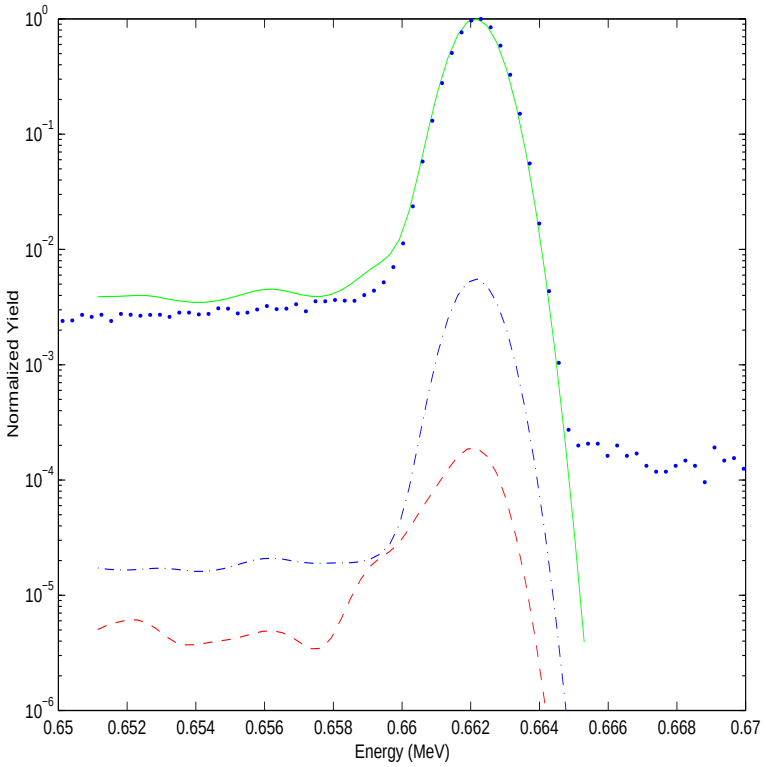

Figure 15: Exponential Tail Components for Ge Detector, Cs-137: Experiment (··), Auger Component (−−), Photoelectron Component (−·)

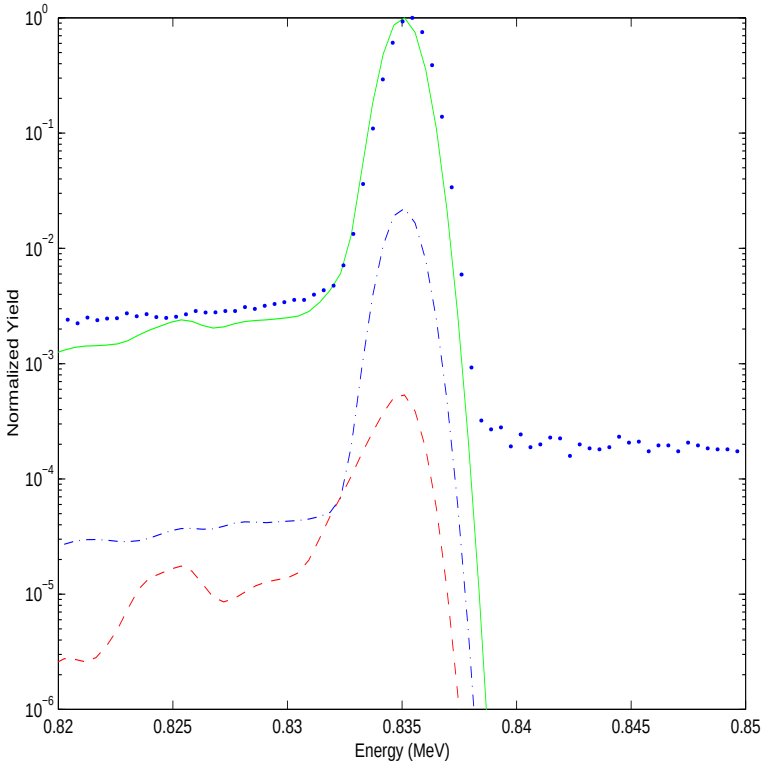

Figure 16: Exponential Tail Components for Ge Detector, Mn-54: Experiment (··), Auger Component (−−), Photoelectron Component (−·)

6.3 Flat Continuum Losses

Electron losses to the sides of the detector create a flat continuum component to the detector response. While Monte Carlo simulation includes electron losses, it underpredicts the magnitude of the loss when comparing with experimental spectra. The difference in magnitude was attributed to an increased loss within the range of the photoelectron. More recent studies indicated that the entire photon spectrum contributed to the shape of the flat continuum.

The components that describe the flat continuum have been calculated by Monte Carlo simulation and subdivided into a Compton electron and photo electron contribution. One of the proposed solutions was to increase the electron leakage artificially by increasing the electron range thus simulating charge loss due to imperfections or electron channeling effects. This could be included in the Monte Carlo simulation by modifying the density of the material for the electron when an electron is created. A treatment that is similar by Geretschlager (1987) assumes an exponential spatial distribution of impurities and reduces the collection efficiency if an interaction occurs within the impurity cluster. Figure 17 demonstrates the effect of including a 'pseudo electron density' modification for a Ge detector at 0.662 MeV. The decreased density increases the electron leakage. Figure 17 shows this by decreasing the density by half the nominal and a tenth the nominal density. This is reflected as the two flat continuum components increase in magnitude. The most significant improvement is in the Compton valley. The density modification could be changed until the Monte Carlo simulation matched the experimental data.

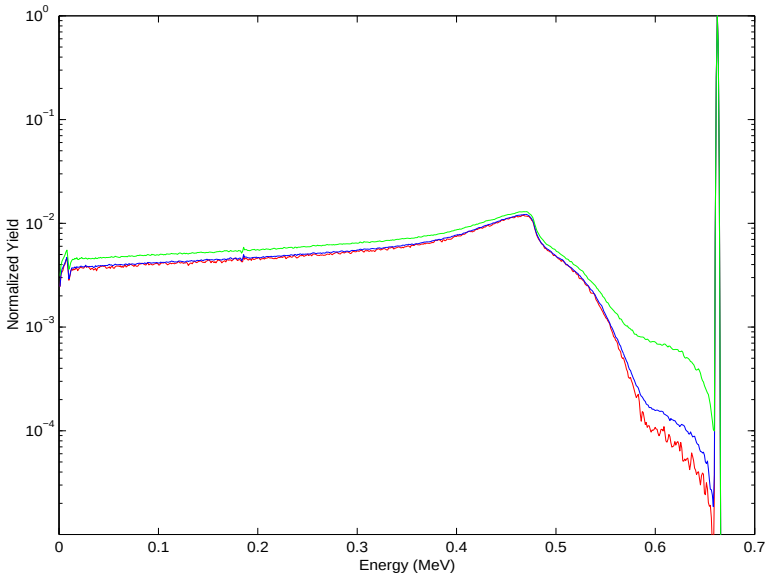

Figure 17: Pseudo electron density modification: $\rho_{nominal}$, $0.5\rho_{nominal}$, and $0.1\rho_{nominal}$

An alternative to this could be to simply reduce the photopeak by a specified fraction and distribute it to the rest of the spectrum. This offers the advantage of a convolution calculation after the basic Monte Carlo simulation that is particular to a specific detector. A program has been written to simulate the increased electron leakage by applying a fraction of the photons that deposit their full energy and simply spreading them equally over the entire spectrum below the energy of interest. It is applied after the Monte Carlo simulation but before the Gaussian convolution. Table 2 gives the applied photo fraction for each detector. Figures 18-23 show the effect of this treatment. A constant value for a specific detector applied to the photopeak appears sufficient to regenerate the distribution. Figures 22 and 23 also show that this convolution does not appear to work well below 100 keV. It should be noted that the photopeak should be generated separately including any low-energy tailing features after this convolution.

Table 2: Applied Photofraction for Flat Continuum

Detector Type	Photo Fraction
SiLi 1	0.70
SiLi 2	0.65
HPGe 1	0.40
HPGe 2	0.45
NaI	0.08

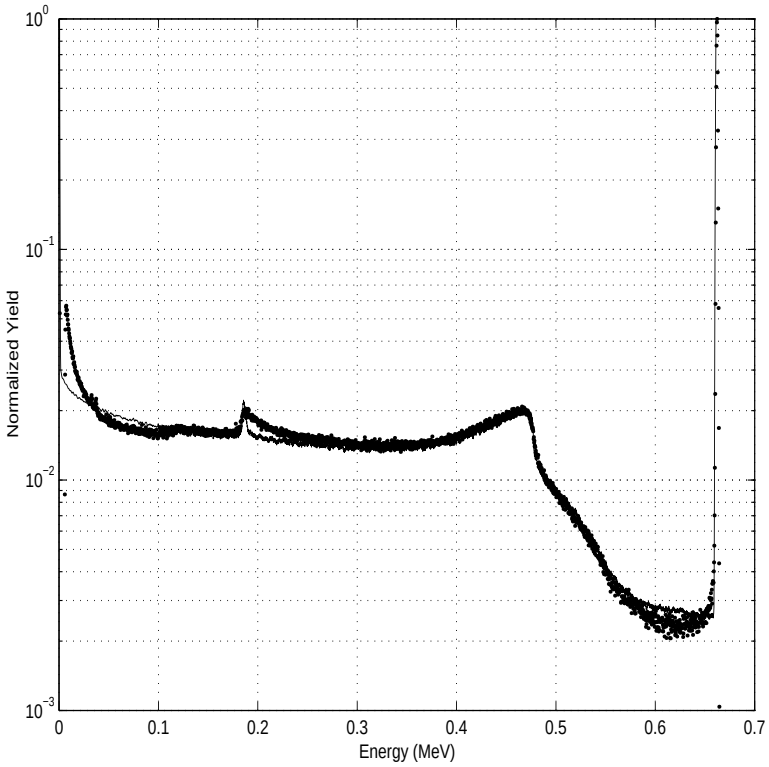

Figure 18: Flat Continuum Results for HPGe #1, Cs-137: Experiment (··), Flat continuum convolution(−)

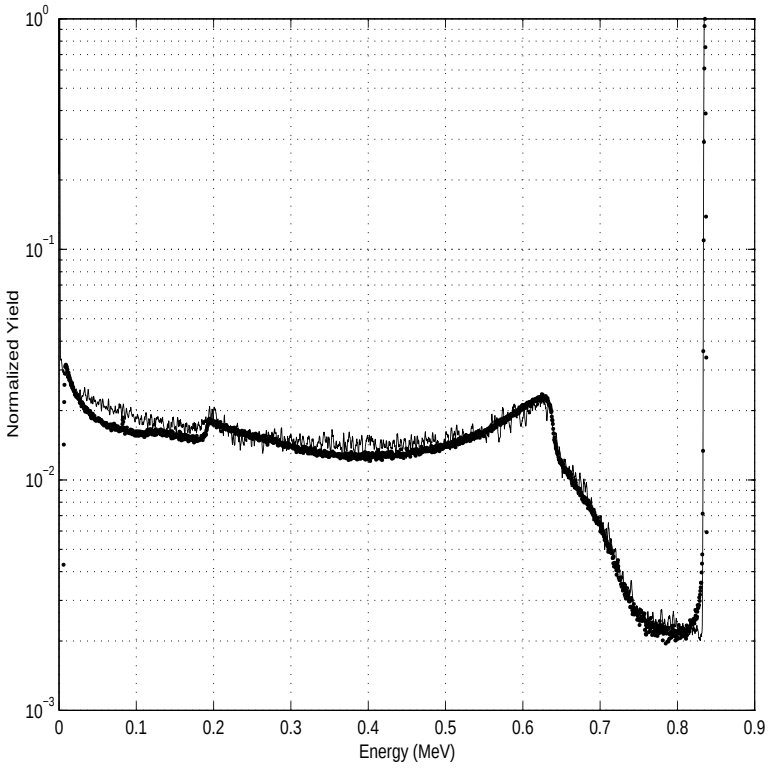

Figure 19: Flat Continuum Results for HPGe #1, Mn-54: Experiment (··), Flat continuum convolution(−)

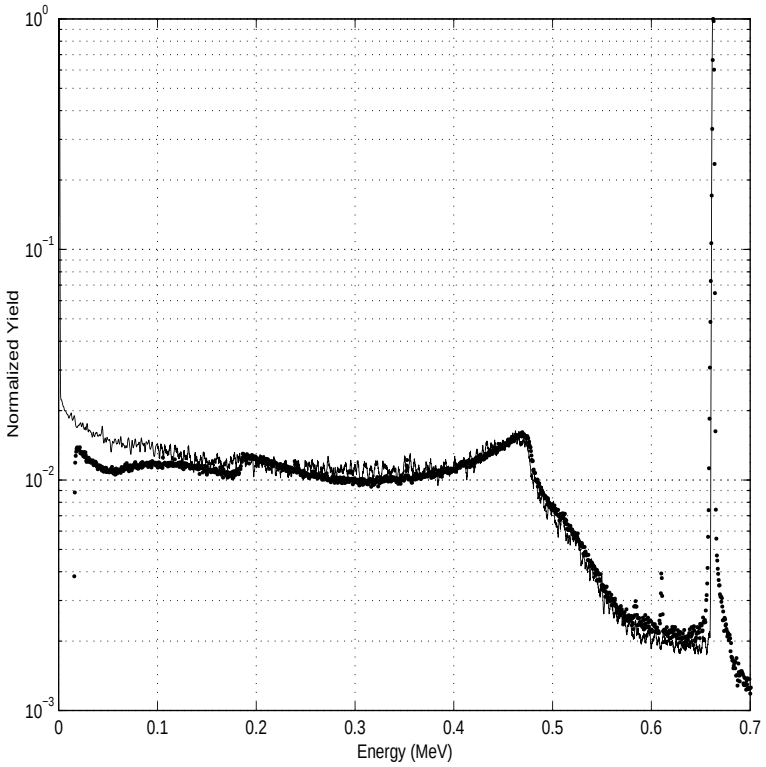

Figure 20: Flat Continuum Results for HPGe #2, Cs-137: Experiment (··), Flat continuum convolution(−)

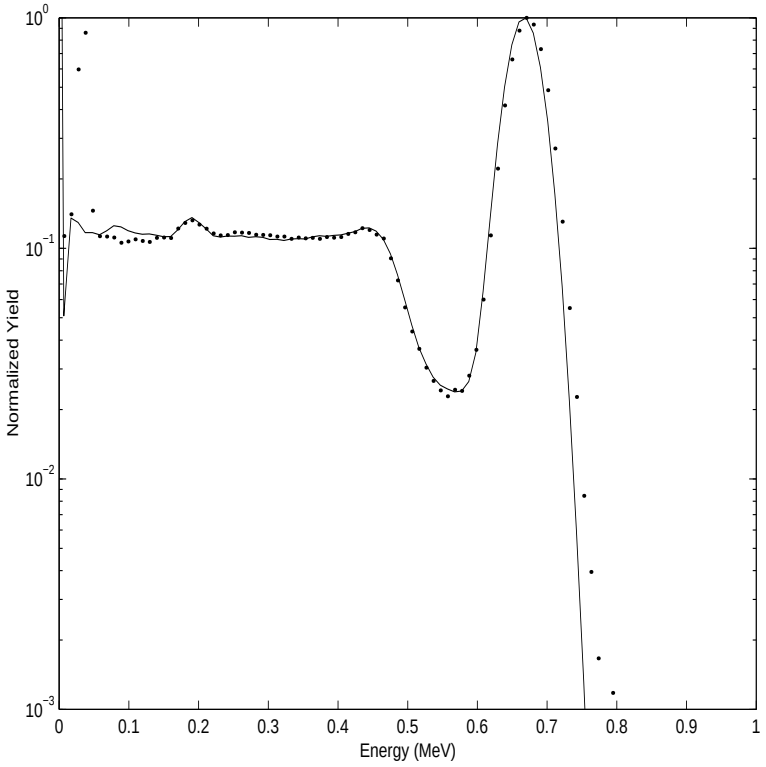

Figure 21: Flat Continuum Results for NaI, Cs-137: Experiment (··), Flat continuum convolution(−)

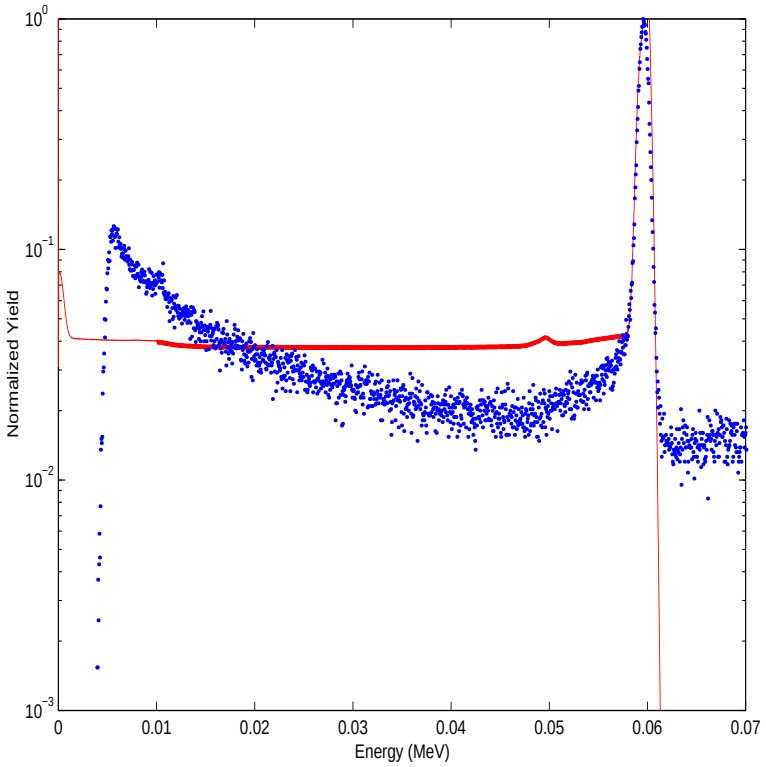

Figure 22: Flat Continuum Results, HPGe #2, Am-241: Experiment (··), Flat continuum convolution(−)

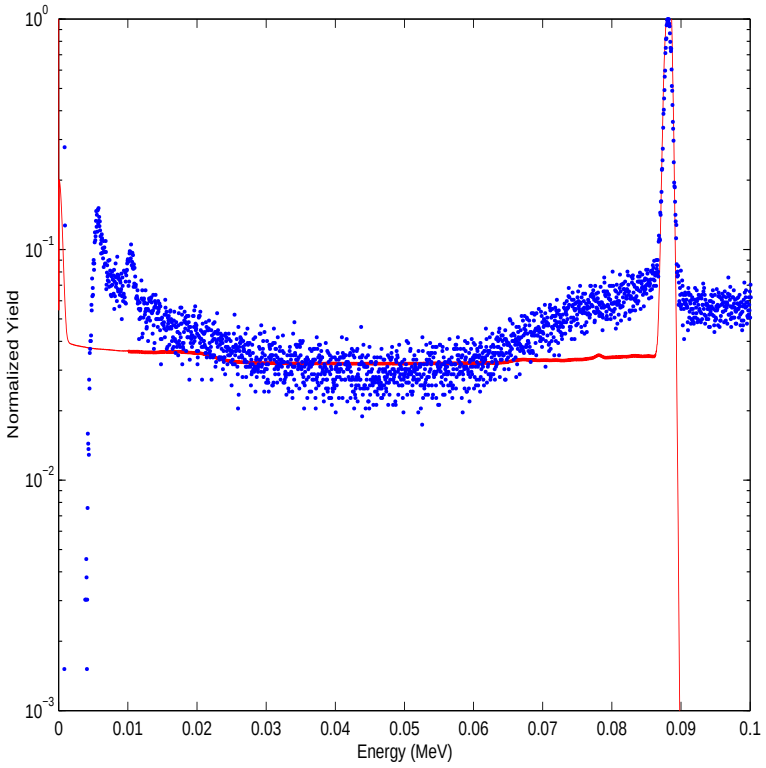

Figure 23: Flat Continuum Results, HPGe #2, Cd-109: Experiment (··), Flat continuum convolution(−)

7 Detector Response Function Validation

It has been shown that Monte Carlo simulation can reproduce many of the features of the detector response function. However, there are features particular to each detector that are nearly impossible to determine and cannot be simulated. Generating these characteristics by Monte Carlo is not practical and should be augmented with separate programs that are used to match a limited number of experimental single energy spectra. This work has concentrated on the possible physical mechanisms that produce the correct shape and magnitude of the Compton edge, the exponential tails and the flat continuua. The Monte Carlo simulation has been improved to include Doppler motion and supplimentary codes have been developed to generate the exponential tails and flat continuua.

An advantage of generating detector response functions with Monte Carlo simulation instead of semi-empirical methods is the reduction in the number of monoenergetic experimental spectra required to validate the results. Table 3 summarizes the experimental data taken from the Heath catalogues (1964, 1974) and from detectors at NCSU that were chosen to reproduce using these techniques. Figures 24-35 show the comparison of experimental data and calculated response. The calculated response represents the combination of the Monte Carlo generated spectra with the convolution of the flat continuum and the addition of the photopeak shape with a Gaussian convolution of appropriate resolution.

The agreement is good for most detectors. However, there is concern for energies below 100 keV for the high purity Ge detectors. The experimental data for these

Table 3: Experimental Data

Detector	Isotope	Energy (keV)
SiLi 1	Fe--55	5.89
	Mo--93	17.4
	Cd--109	88.1
SiLi 2	Cd--109	88.1
HPGe 1	Am--241	59.5
	Cd--109	88.1
	Cs--137	662
HPGe 2	Cs--137	662
	Mn--54	835
NaI	Be--7	478
	Cs--137	662
	Mn--54	835

energies was taken at NCSU with a point source and contain low-energy contributions from other gamma emissions at higher energies. These particular energies represent the lower limit of detection for Ge detectors and the upper limit for SiLi detectors. The experimental spectra for the SiLi detectors does not reproduce the flat continuum accurately. This is due to the multiple X-ray energies emitted by the radioisotope source.

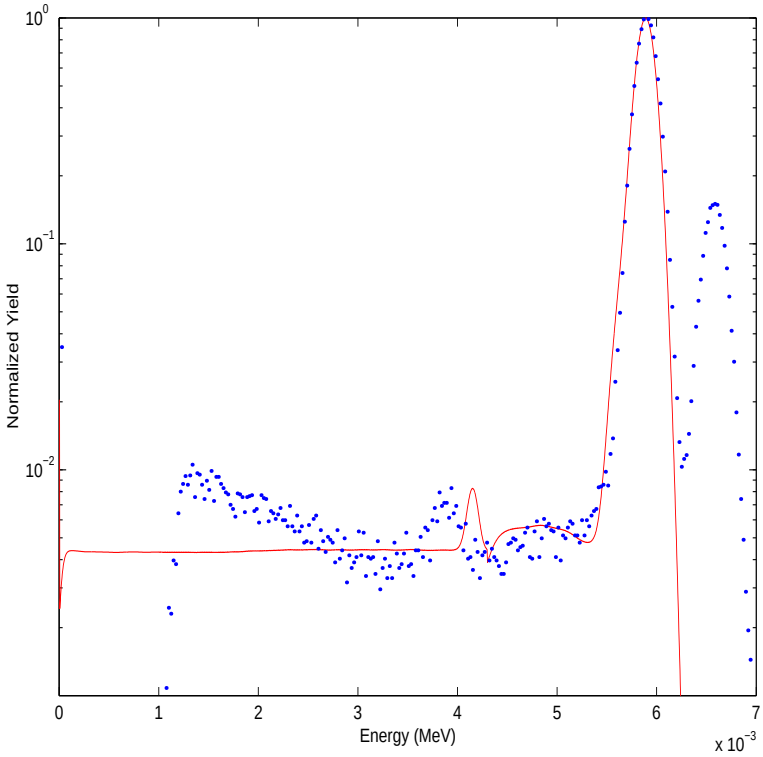

Figure 24: SiLi #1, Fe-55: Experiment (··), Monte Carlo generated response(−)

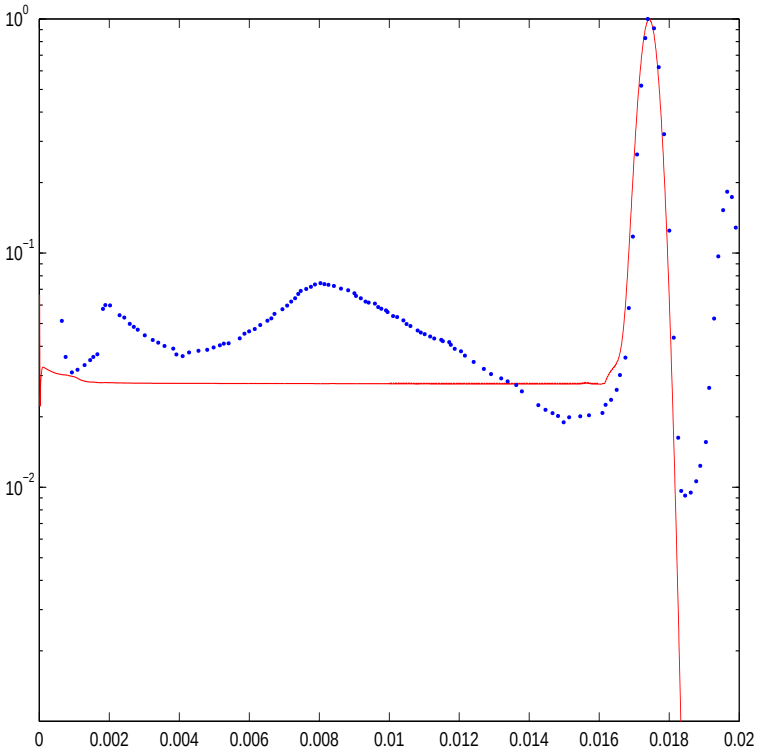

Figure 25: SiLi #1, Mo-93: Experiment (··), Monte Carlo generated response(−)

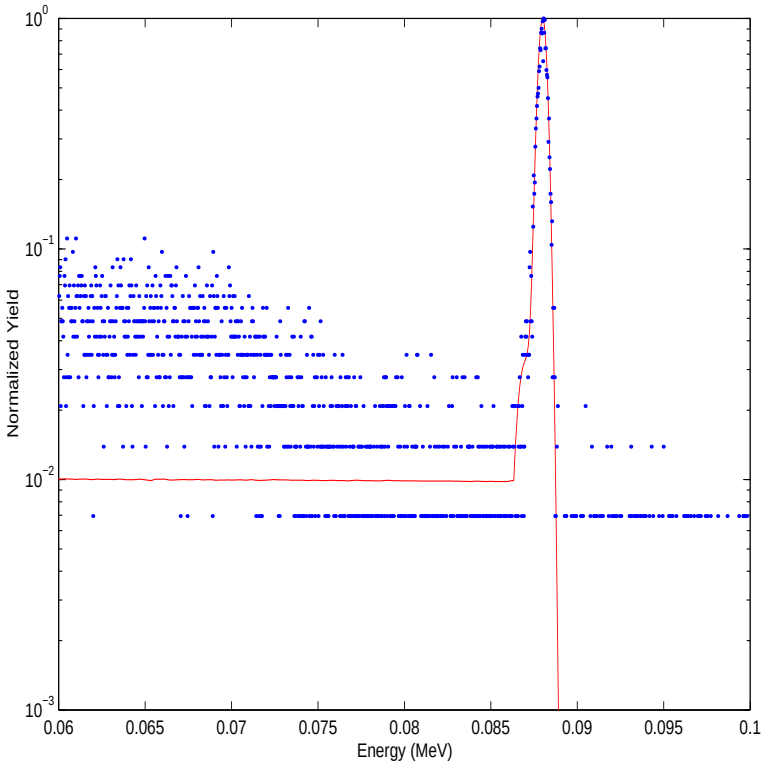

Figure 26: SiLi #1, Cd-109: Experiment (··), Monte Carlo generated response(−)

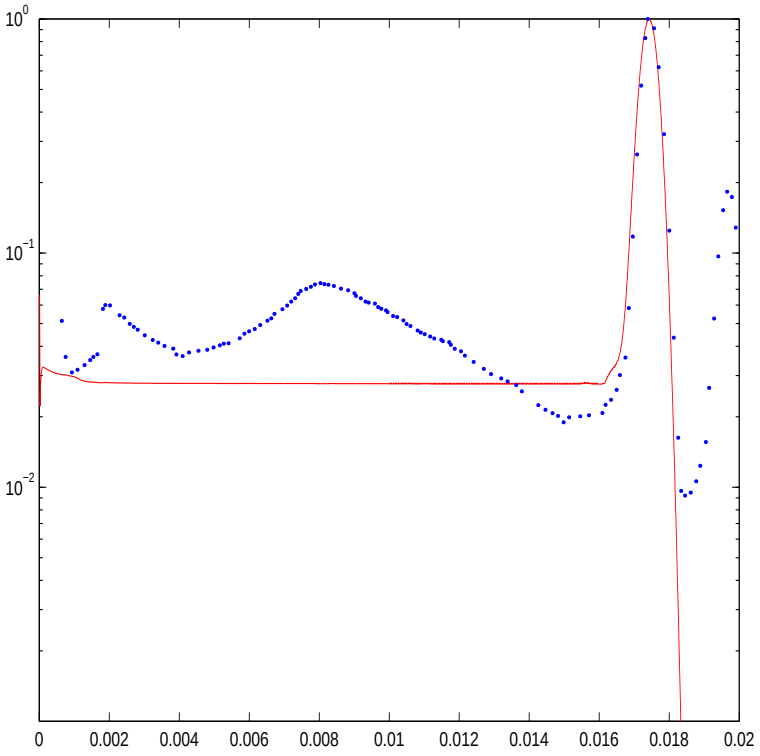

Figure 27: SiLi #2, Cd-109: Experiment (··), Monte Carlo generated response(−)

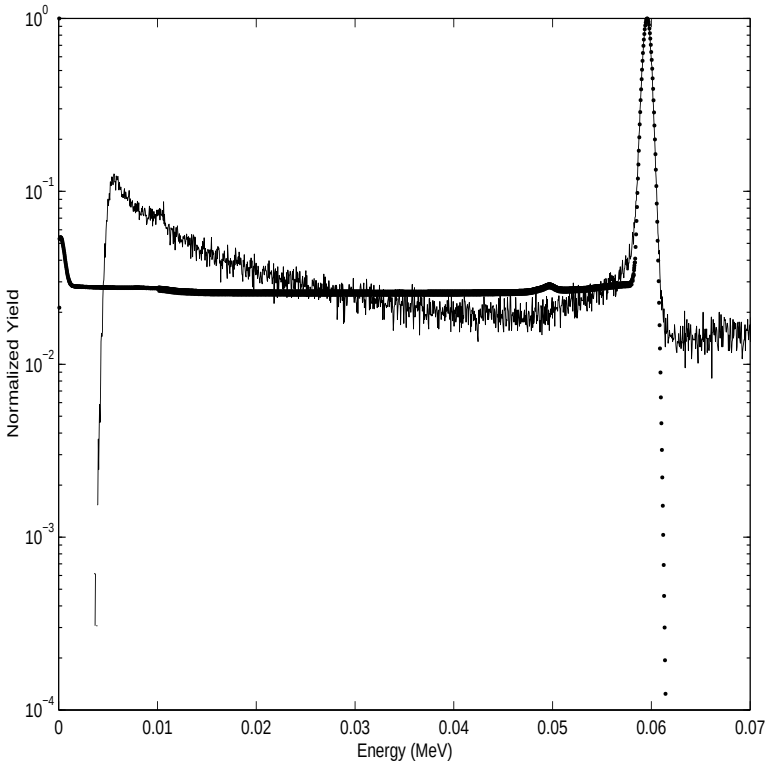

Figure 28: HPGe #1, Am-241: Experiment (··), Monte Carlo generated response(−)

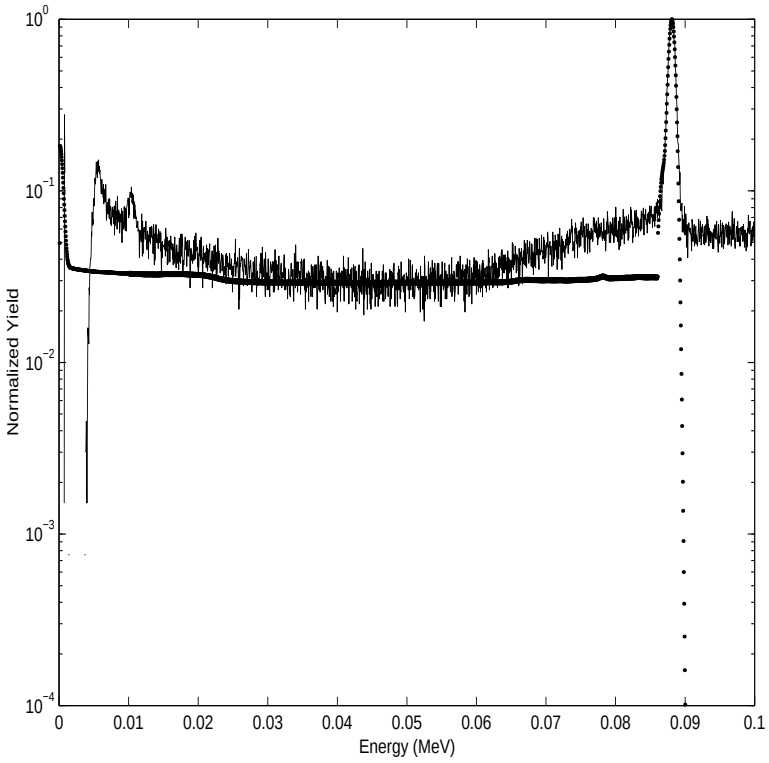

Figure 29: HPGe #1, Cd-109: Experiment (··), Monte Carlo generated response(−)

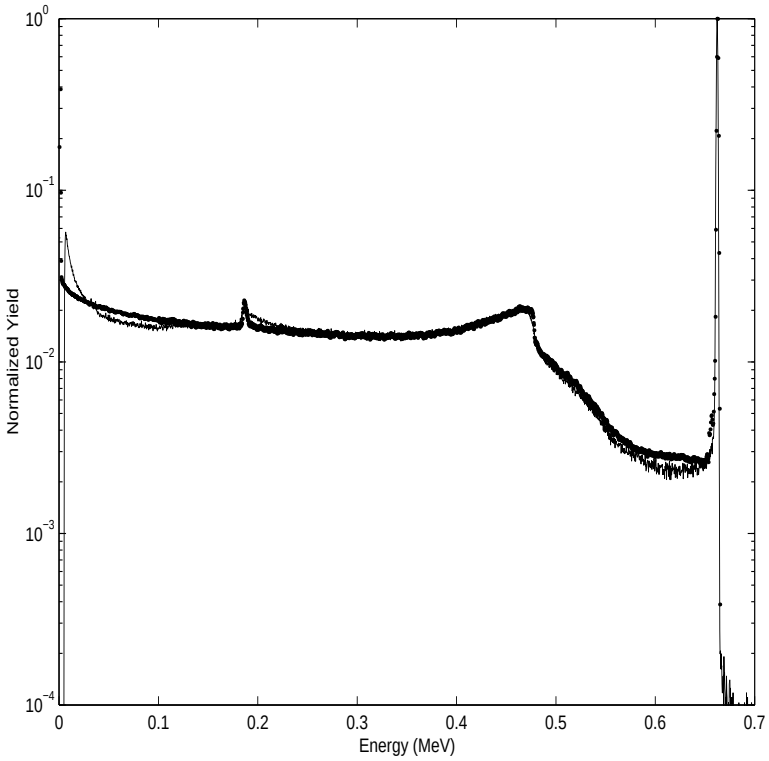

Figure 30: HPGe #1, Cs-137: Experiment (··), Monte Carlo generated response(−)

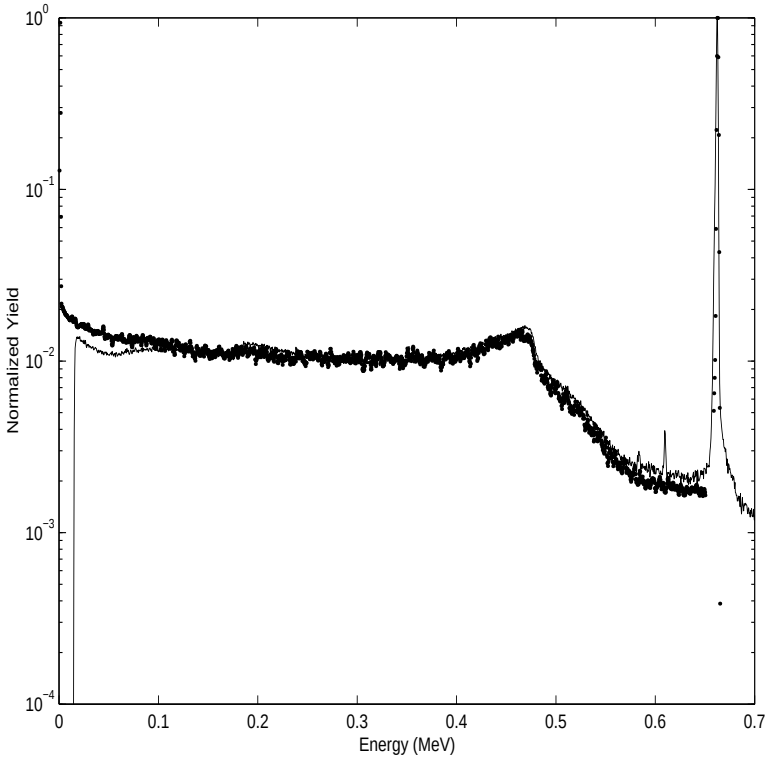

Figure 31: HPGe #2, Cs-137: Experiment (··), Monte Carlo generated response(−)

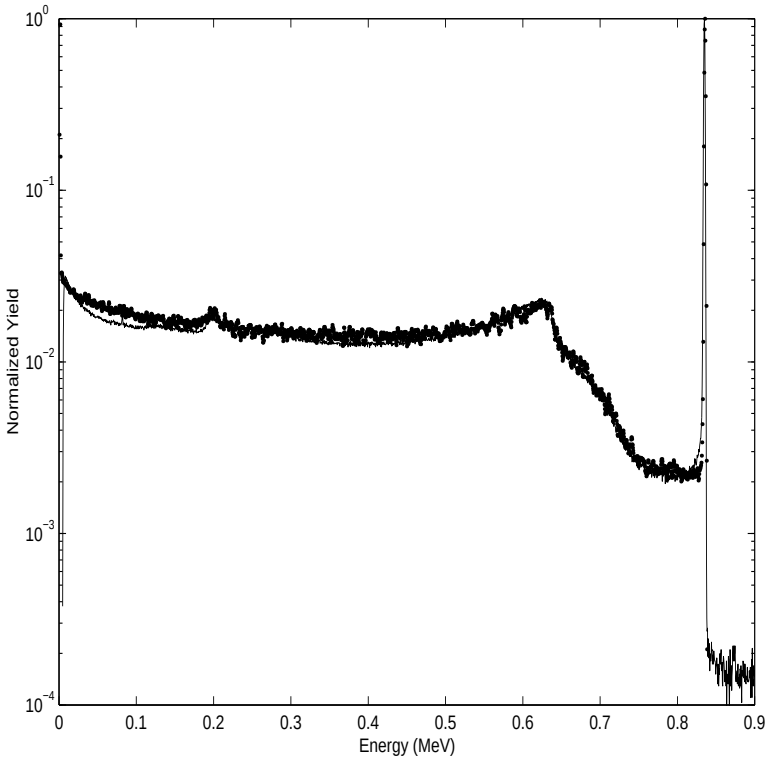

Figure 32: HPGe #2, Cs-137: Experiment (··), Monte Carlo generated response(−)

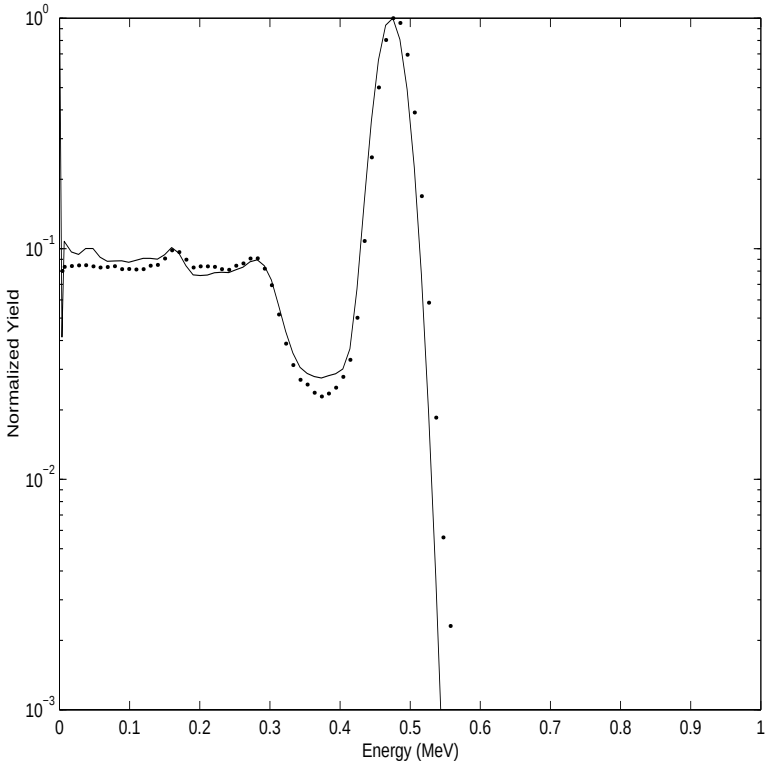

Figure 33: NaI, Be-7: Experiment (··), Monte Carlo generated response(−)

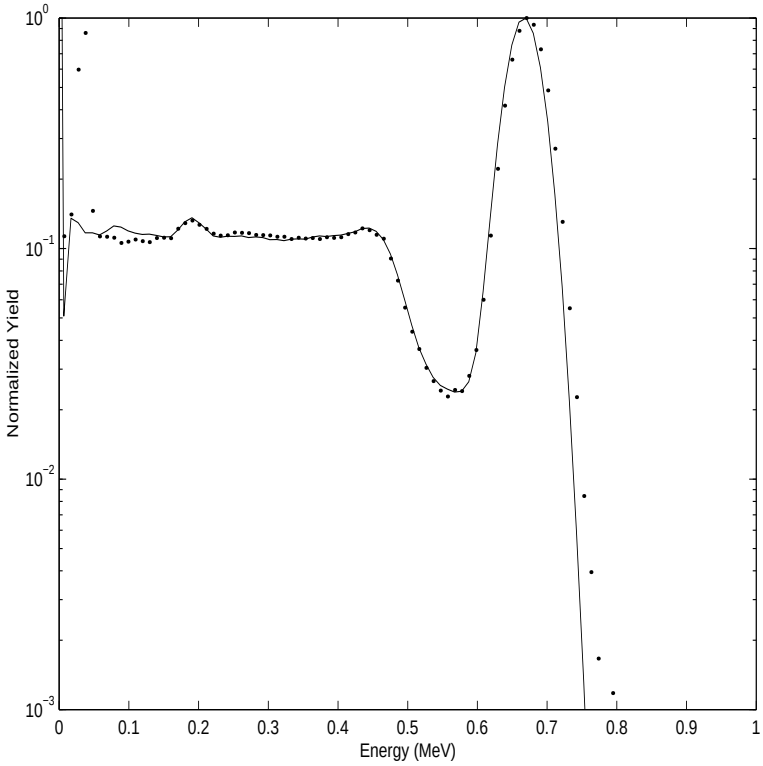

Figure 34: NaI, Cs-137: Experiment (··), Monte Carlo generated response(−)

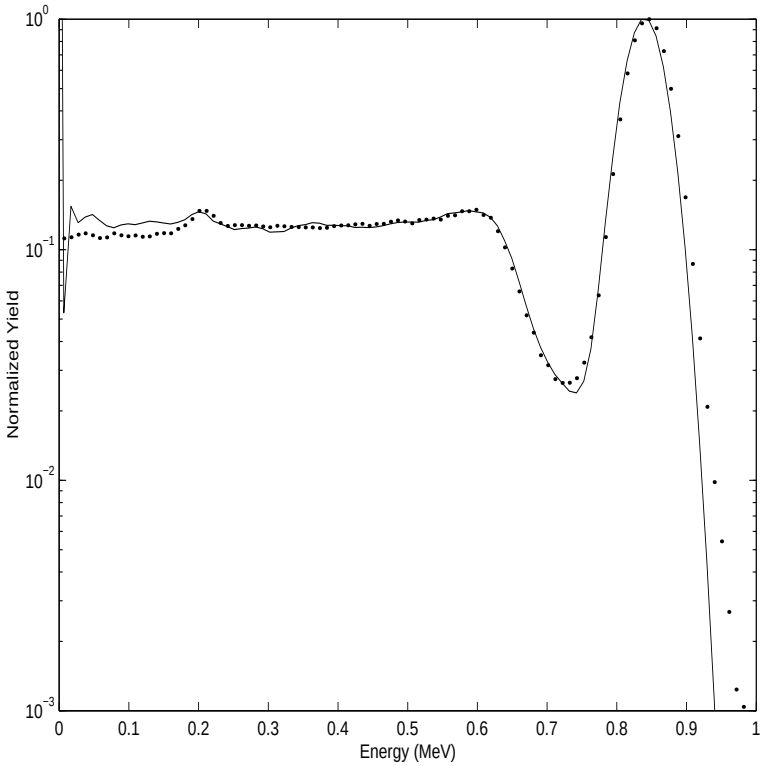

Figure 35: NaI, Mn-54: Experiment (··), Monte Carlo generated response(−)

8 Summary and Conclusions

There are several features of the detector response function that have required improvement. The ideas presented here affect the fundamental components of detector response. Through the use of Monte Carlo simulation, the shape of the fundamental physical mechanisms that produced the detector response have been described. One area that required improved accuracy is the shape of the Compton edge. The shape is dominated by the first and second Compton scatters which previously neglected the change in photon energy and angle due to the momentum imparted by the Doppler motion of the bound electron. This work utlized the methods developed by Namito (1993) and incorporated Doppler motion into the Monte Carlo simulation. Doppler motion is currently not treated in most general purpose Monte Carlo codes with the recent exception of a special version of EGS4 (Namito, 1993) but is now included in a local version of MCNP4B.

The next two areas that required improvement are in the valley region between the Compton edge and the photopeak and the Compton continua. The imperfections in the detector crystal serve as electron trapping sites and thus increase the amount of incomplete charge collection. The resulting effect is similar to electron losses from the surface of the detector crystal. Since this detector characteristic cannot be physically described, an approximation was made. A convolution program has been written to simulate the increased electron leakage by applying a fraction of the photons that deposit their full energy and simply spreading them equally over the entire spectrum below the energy of interest. This offers the advantage of a convolution after the basic

Monte Carlo simulation that is particular to a specific detector and is applied after the Monte Carlo simulation but before the Gaussian convolution.

The next area of improvement was in the exponential tail that appears left of the main photopeak. Previous authors' conclusions in the literature were matched independently. The frontal region of the detector is unusually significant to the shape of the photopeak. The tailing feature is greatly enhanced when there is a contribution from an inactive region. A general description of a dead layer and a region of poor charge collection was described by using a pseudo density correction when an electron was created. The parameters of this model allow simulation for different detectors of the same material. Also, simulation results only show the exponential behavior when a full description of the de-excitation process is included. This included Auger electrons, satellite Auger X-rays, and fluorescence X-rays. General agreement with experimental data is reached. The shape of this feature resembles the previous short and long term exponentials used in semi-empirical methods. Further refinement of the pseudo-density model should be pursued.

The methods described here are applicable to any scintillation or semi-conductor detector systems and were used specifically for NaI, Ge, and Si detectors. The availability of completely described benchmark quality data is essential to the experimental validation of these methods. Fortunately, this has been solved for NaI and HPGe detectors by the work of Heath, however, there is not a consistent set of benchmark quality data for Si detector systems. This may be solved by generating data with the help of mono-energetic photons originiating from linear accelerators or synchotron radiation sources

9 References

1. Berger, M.J., and Seltzer, S.M., 1972, Response Functions for Sodium Iodide Scintilation Detectors. Nuclear Instruments and Methods, Vol 104, 317-332.

2. Biggs, F., Mendelsohn, L.B. and Mann, J.B., 1975, Atomic Data and Nuclear Data Tables, Vol. 16, 201-309.

3. Briesmeister, J. F. (1997), MCNP - A general purpose Monte Carlo n-particle transport code version 4b, LA-12625-M.

4. Campbell, J.L., 1990, X-Ray Spectrometers for PIXE. Nuclear Instruments and Methods in Physics Research, B49, 115-125.

5. Carter, L.L., and Cashwell, E.D., 1975, Particle Transport Simulation with the Monte Carlo Method, ERDA Critical Review Series, TID 26607.

6. Chun, R., Gadeken, L.I., and Roberson, B.C., 1976, Multiple Interaction Processes in Ge(Li) Detector Pulse Formation. Nuclear Instruments and Methods, Vol 137, 295.

7. Felsteiner, J, Pattison, P., and Cooper, M., 1974, Effects of Multiple Scattering on Experimental Compton Profiles: a Monte Carlo Calculation. Phil. Mag., Vol 30, 537-548.

8. Gardner, R.P., A.M. Yacout, J. Zhang, and K. Verghese, 1986, An Investigation of the Possible Interaction Mechanisms for SiLi and Ge Detector Response Functions by Monte Carlo Simulation. Nuclear Instruments and Methods in Physics Research, A242, 399-405.

9. Geretschlager, M., 1987, Monte Carlo Simulation of the Response of SiLi X-Ray Detectors to Proton Induced K X-Rays of Light Elements ($12 \leq Z \leq 32$) Applied to Efficiency Determination. Nuclear Instruments and Methods in Physics Research, B28, 289-298.

10. Goto, S., 1993, Response Function of a SiLi Detector for Photon Energies from 1 to 10 keV. Nuclear Instruments and Methods in Physics Research, A333, 452-457.

11. Halbleib, J.A. and Mehlhorn, T.A., 1984, ITS: The Integrated TIGER Series of Coupled Electron/Photon Monte Carlo Transport Codes, SNL SAND 84-0573.

12. Hansen, N.E. and Fultz, S.C., 1960, Cross Sections and Spectra for Negative Electron Bremsstrahlung. UCRL-6099.

13. He, T., Gardner, and Verghese, K. 1990, An Improved SiLi Detector Response Function. Nuclear Instruments and Methods in Physics Research A299, pp. 354-366.

14. He, H., Zhang, T., Shang, R. and Xu, S, 1988, Nuclear Instruments and Methods in Physics Research A272, pp. 847.

15. Heath, R.L., 1964, Scintillation Spectrometry, Gamma-Ray Spectrum Catalogue, 2nd Ed, USAEC Report IDO-16880.

16. Heath, R.L., 1974, Ge(Li) and Si(Li) Gamma-ray Spectra, Gamma-Ray Spectrum Catalogue 4th Ed, INEEL.

17. Ingersol, D.T. and Whering, D.W., 1977, Nuclear Instruments and Methods, Vol 147, 551.

18. Jin, Y., R.P. Gardner and Verghese, K., 1986, A Semi-Empirical Model for the Gamma-Ray Response Function of Germanium Detectors Based on Fundamental Interaction Mechanisms. Nuclear Instruments and Methods in Physics Research, A242, 416-426.

19. Keyser, R.M. and Raudorf, T.W., 1990, Germanium Radiation Detector Manufacturing: Process and Advances. Nuclear Instruments and Methods in Physics Research, A286, 357-363.

20. Knoll, G.F., 1989, Radiation Detection and Measurement. John Wiley and Sons, Inc., New York.

21. Krause, M.O., 1979, Atomic Radiative and Radiationless Yields for K and L Shells. J. Phys. Chem, Ref. Data, Vol 8, 307.

22. Lee, M.C., K. Verghese, and Gardner,R.P., 1987, A Semiempirical Germanium Detector Response Function for 0.06- to 6.1 MeV Gamma Rays. Transactions of the American Nuclear Society, Vol. 55, 555-557.

23. Lee, M.C. K. Verghese, and Gardner R.P., 1987, Extension of the Semi-Empirical Germanium Detector Response Function to Low Energy Gamma Rays. Nuclear Instruments and Methods in Physics Research, A262, 430-438.

24. Lee, S.H., Ph.D Thesis, NCSU.

25. Mayo, R.M., 1998, Introduction to Nuclear Concepts for Engineers. American Nuclear Society, La Grange Park Il.

26. Meixner, C.H., 1974, A Monte Carlo Program for the Calculations of Gamma-Ray Spectra for Germanium Detectors. Nuclear Instruments and Methods, Vol 119, 521.

27. Nakamura, T., 1975, Monte Carlo Calculation of Peak Efficiencies and Response Functions of Coaxial-type Ge(Li) Detectors for Disk Gamma-Ray Sources. Nuclear Instruments and Methods, Vol 131, 521.

28. Namito, Y., Ban, S., and Hirayama, H., 1993, Implementation of the Doppler Broadening of a Compton-Scattered Photon into the EGS4 Code. Nuclear Instruments and Methods in Physics Research, A332, 270-283.

29. Pages, L., Bertel, E., Joffre, H., Sklavenitis, L., 1972, Energy Loss, Range and Bremsstrahlung Yield for 10 keV to 100 MeV Electrons. Atomic Data Vol 4, 79.

30. Papp, T., Campbell, J.L., Varga, D., Kalinka, G., 1998, An Alternative Approach to the Response Functino of Si(Li) X-ray Detectors Based on XPS Study of Silicon and Front Contact Materials. Nuclear Instruments and Methods in Physics Research A412, 109-222.

31. Pasic, S., Ilakovac, K, 1998, Measurement of the Component of the Ge Detector Response Functino Due to Escape of Secondary Radiation. Nuclear Instruments and Methods in Physics Research A405, 45-52..

32. Peplow, D.E., R.P. Gardner, and K. Verghese, 1994, Nuclear Geophysics, Vol. 8, No. 3, pp. 243-259.

33. Peplow, D.E., 1993, MS Thesis, NCSU.

34. Rogers, D.W.O., 1982, More Realistic Monte Carlo Calculations of Photon Detector Response Functions. Nuclear Instruments and Methods, Vol 199, 531.

35. Scofield, J.H., 1974, Atomic Data and Nucl. Data Tables, Vol 14, 121.

36. Seltzer, S.M., 1981, Calculated Response of Intrinsic Germanium Detectors to Narrow Beams of Photons with Energies up to Approximately 300 keV. Nuclear Instruments and Methods, Vol 188, 133.

37. Storm, E. and Isreal, H.I., 1967, Photon Cross Sections from 0.001 to 100 MeV for Elements 1 through 100., LASL report LA-3753.

38. Yacout, A.M., R.P. Gardner and K. Verghese, 1986, A Semi-Empirical Model for the X-Ray SiLi Detector Response Function. Nuclear Instruments and Methods in Physics Research, A243, 121-130.

39. Wang, J.X, and Campbell, J.L., 1991, Monte Carlo Simulation of the Response of SiLi Detectors to Monoenergetic X-rays. Nuclear Instruments and Methods in Physics Research, Vol B54, 499.

40. Wang, J.X, and Campbell, J.L., 1992, X-Ray Spectrometry Vol 21, 223.

41. Wang, Y.Y. 1996, MS Thesis, NCSU.

42. Wainio, K.W. and Knoll, G.F., 1966, Calculated Gamma-Ray Response Characteristics of Semiconductor Detectors. Nuclear Instruments and Methods, Vol 44, 213.